To the Graduate Council:

I am submitting herewith a thesis written by Melvin Bruce Rohrbaugh Jr. entitled "Estimating Joint Intensity, Density and Mean Tracelength using Circular Scanlines and Circular Windows." I have examined the final copy of this thesis for form and content and recommend that it be accepted in partial fulfillment of the requirements for the degree of Master of Science, with a major in Geology.

William M. Dunne

William M. Dunne, Major Professor

Matthew Mauldon

Matthew Mauldon, Major Professor

I have read this thesis and recommend its acceptance:

Robert D. Hatcher, Jr.

Robert D. Hatcher, Jr.

Accepted for the Council:

C W Minkel

Associate Vice Chancellor and
Dean of The Graduate School

ESTIMATING JOINT INTENSITY, DENSITY AND MEAN TRACELENGTH USING CIRCULAR SCANLINES AND CIRCULAR WINDOWS

A Thesis
Presented for the
Master of Science
Degree
The University of Tennessee, Knoxville

Melvin Bruce Rohrbaugh Jr.
May 2000

This thesis is dedicated to my parents,

Melvin and Josephine Rohrbaugh

ACKNOWLEDGEMENTS

This research would not have been possible without the partial funding from the donors of the Petroleum Research Fund, administered by the ACS; Geological Society of America; and the Southeastern section of the Geological Society of America. I would like to thank my co-advisors, Dr William M. Dunne (Dept. of Geological Sciences) and Dr Matthew Mauldon (Dept. of Civil & Environmental Engineering), for their guidance and patience throughout the course of my research. Also, I would like to thank both of you for allowing me to work on a thesis that allowed me to integrate both my geology and computer programming skills. I also thank my other committee member, Dr. Robert D. Hatcher, Jr., for his assistance during this research.

For the programming aspect of my thesis, I would like to thank You Li for helping me learn some of the nuances of the Visual Basic language. Yen-Yit Chan and Jim Calcagno are thanked for helping me solve the little, but pesky, problems that occurred during programming. Last, but certainly not least, I would like to thank Camilo Montes for his programming assistance. Without your help, I would have never figured out how to import digitized natural patterns from Adobe Illustrator® into JAWS.

I would like to thank James Hogan for all the long, long conversations about SEINFELD, school, research, sports, etc. It's been fun. Also, let us not forget about all the negative encouragement. Wendy Lawdermilk, thanks for all the Aggie propaganda and animal crackers. Now that I am gone, you have unlimited computer time, and the little filing cabinet.

I would also like to thank all the rest of my friends in the department, Alan Spraggins, the "Hatchery", the "West Georgia Pod", Mike Wyatt, Heather Gastineau, Elizabeth Humbert, Janna Peevler, Amy Robinson, Marvin Bennett, just to name a few. All of you have made this an enjoyable experience.

Last, but certainly not least, I want to thank my parents for allowing me to pursue my dreams, wherever they took me. Without your encouragement, this degree would not have been possible.

ABSTRACT

The purpose of this thesis is to evaluate and demonstrate the performance of new circular scanline and circular window estimators of joint intensity, density and mean tracelength. The estimators are distribution independent and provide a rapid means of estimating parameters, because only counts of fracture trace intersections and/or trace endpoints are needed. These estimators defeat the problems of orientation bias, censoring and length bias, which plagued previous methods. Using synthetic patterns with known parameters, the estimators reliably match control values. When applied to nine different joint sets or pavements, the estimators also correctly estimate fracture characteristics. A 95% prediction interval is used to establish confidence in measurements by defining the likely range for new predicted values. Plots for prediction interval show that the interval for predicted values is reduced and hence, estimate quality improved more efficiently by using sampling schemes that increase radius rather than number of circles. Larger circles are more efficient because they effectively average out spatial heterogeneity. When estimating mean tracelength, reliability of estimates is also improved by sampling schemes that yield large counts of fracture endpoints. Analysis of synthetic patterns shows that for trace centers described by a Poisson process, sampling schemes that capture 20 endpoints, on average, are needed to produce reliable results. This value should not be applied literally to natural patterns, as they are not typically Poissonian, but this analysis emphasizes the benefits of large sample size. These estimators may be applied to any type of data set that consists of linear traces, including fault traces on a planar slice through a 3-d seismic reflection data cube.

TABLE OF CONTENTS

LIST OF TABLES

LIST OF FIGURES

1. INTRODUCTION

The purpose of this thesis is to evaluate and demonstrate the performance of new estimators for joint intensity, density and mean tracelength utilizing circular scanlines and circular windows as measurement tools (Mauldon, 1998; Mauldon et al., 1999a, b). By estimating these parameters in fractured rock volumes, geoscientists can more accurately assess hydrocarbon flow and storage (Reiss, 1982; Nelson, 1985; Dershowitz and LaPointe, 1994; Narr, 1996), groundwater flow and storage (Long and Witherspoon, 1985; Bear et al., 1993; McKay et al., 1993; Anna and Wallman, 1997), slope stability (Hoek and Bray, 1977), rockmass mechanical behavior (Jaeger and Cook, 1969; Goodman and Shi, 1985; Amadei and Savage, 1993; Kulatilake et al., 1993a), and elastic rock properties (Segall and Pollard, 1983; Fossum, 1985; Hu and Huang, 1993). The quality of the new circular scanline/window estimators will be evaluated for both synthetic and natural patterns. This approach will be used to (1) confirm that the estimated values tend toward the true values for the underlying population of joint traces; (2) compare the performance of these new estimators to existing estimators; (3) establish 95% confidence levels for predictions from applying the estimators; and (4) determine the minimum sample size for which the mean tracelength estimator will reliably estimate mean tracelength.

Fracture Characteristics

Fracture density in the past has often been treated as identical to the apparent density, i.e., the number of fractures observed per unit volume, area or length (Dershowitz and Herda, 1992; Ghosh and Daemen, 1993). Apparent density, however, which in two dimensions is defined as the number of fractures per unit area, overestimates the true density (Kulatilake and Wu, 1984b; Mauldon, 1994). The magnitude of the overestimate decreases as the sample size increases (Figure 1A, B). For example, set 1 in Figure 1A has an apparent density of 0.0020 m^{-2} for a circular window of radius 25 m. The estimate decreases to 0.0014 m^{-2} for a radius of 75 m, which more closely approximates the true density of 0.0010 m^{-2}. Obtaining the true density requires identifying unique points, such as centers or terminations on the fractures. Only those fractures with the unique points exposed in the sample region are counted. For example, if centers are counted to determine density for set 1, the estimate is 0.0011 m^{-2} for a circle of radius 25 m and 0.0010 m^{-2} for radius 75 m. Compared to the apparent densities, these estimates are more accurate and show little sensitivity to window size. In natural exposures, centers are typically difficult to identify. Terminations are easier to deal with as will be done in this work.

Fracture size can be defined in three, two or one-dimension, where size denotes fracture volume, area and tracelength, respectively. Typically, only tracelength is measured for joints because it may be directly observed (Figure 1A), whereas joint areas and volumes usually cannot.

Fracture intensity is a pattern characteristic that incorporates both the number and size of the fractures. The most desired measure of fracture intensity is volumetric intensity, defined as the area of fractures per unit volume of rock (Wheeler and Dixon, 1980; Dershowitz and Einstein, 1988; Dershowitz and Herda, 1992; Mauldon, 1994).

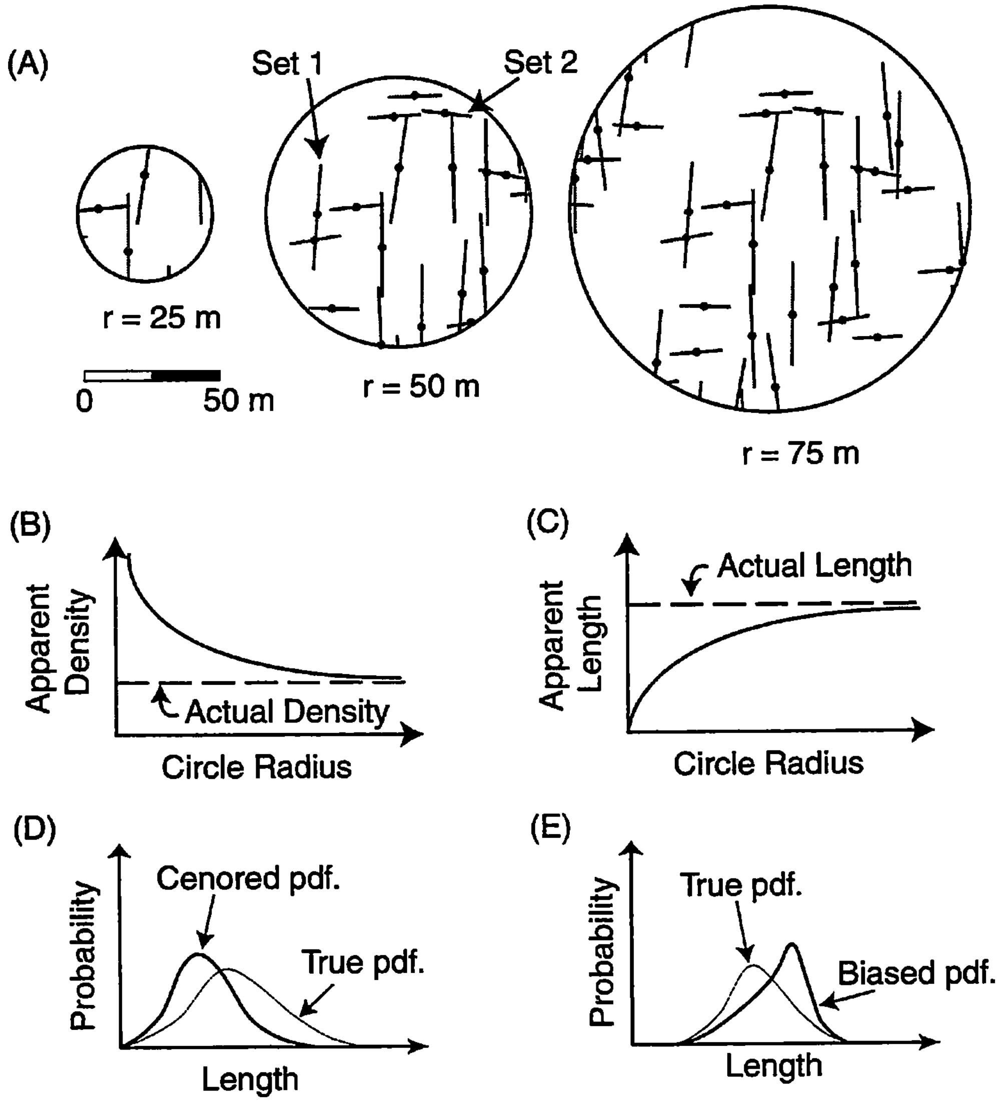

Figure 1- Problems due to censoring and length bias when sampling fracture traces. (A) Same fracture pattern with two sets sampled by three progressively larger circles (dots represent fracture centers). (B) Apparent density overestimates for smaller samples due to censoring and length bias. (C) Mean trace length underestimated due to censoring. (D) Undersampling of joint trace lengths due to censoring as shown by the probability distribution function (pdf). (E) Oversampling of longer traces due to length bias as shown by the pdf.

Volumetric intensity maybe used to determine fracture porosity, when fracture aperture is known, but, since volumetric joint intensity cannot easily be observed without rockmass disaggregation, this measure is not easily obtained. Instead, a pair of dimensionally similar but measurable characteristics are used: areal intensity, defined as the length of fracture traces per unit area of a planar sampling region (Dershowitz and Herda, 1992; Mauldon, 1994; Ehlen, 1998); and linear intensity, defined as the number of fractures per unit length of scanline or borehole (linear intensity) (Priest and Hudson, 1981; Lacazette, 1991; Dershowitz and Herda, 1992; Mauldon, 1994; Becker and Gross, 1996). Volumetric intensity can then, in principle, be extrapolated from linear or areal intensity measurements (Dershowitz and Herda, 1992; Mauldon, 1994). It should be noted that intensity is the product of density and size, unless density and size are correlated variables (e.g., Ang and Tang, 1975).

Current Measurement Methods and Sampling Biases

As joints are commonly observed along lines or surfaces, two common sampling methods exist for estimating intensity, density and mean tracelength: straight scanlines and areal sampling (Figure 2) (LaPointe and Hudson, 1985; Priest, 1993; Wu and Pollard, 1995). Straight scanlines sample the fractures that intersect the scanline and may be used to systematically record number, orientation, aperture, semi-tracelength, etc. (Priest and Hudson, 1981). The area method samples joints that intersect a surface area and usually involves mapping the joint pattern (Wu and Pollard, 1995). Number, tracelength, orientation, aperture, tracelength, etc. may be recorded for all observed joint traces.

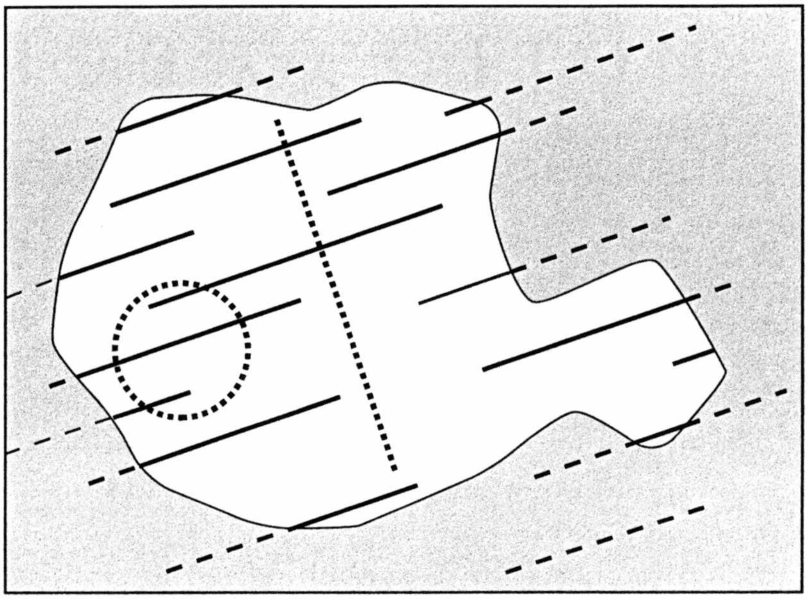

Figure 2 - Straight scanline (thick dotted line), areal sampling (irregular joint pavement window), and a circular scanline/window (thick dotted circle) sampling of a population of joints. Solid lines represent visible joint traces, and dashed lines represent covered portions of joint traces.

A key issue for quantifying characteristics of a joint pattern with samples from straight scanlines or areas is avoiding sampling biases that skew measured values from true values. Sampling biases due to orientation bias, censoring, length bias, and pattern heterogeneity (Baecher and Lanney, 1978; LaPointe and Hudson, 1985) are discussed at length in this thesis.

Orientation bias results if a straight scanline or the long axis of an inequant sampling area is not normal to a joint set (Terzaghi, 1965; Priest, 1993; Mauldon and Mauldon, 1997). For parallel joints, intensity estimates from scanlines can be corrected by dividing by cos α, where α is the angle between the scanline and the normal to the joint set (Terzaghi, 1965). This correction factor, however, produces spurious results as α approaches 90°, and equals infinity when α is 90° (Terzaghi, 1965; Mauldon and Mauldon, 1997). To reduce the effects of this correction artifact, arbitrary upper limits for the correction factor of 10° to 20° have been proposed (Yow, 1987; Priest, 1993).

Censoring occurs for joints that extend beyond the visible exposure, so that one or both ends of the joint cannot be seen (Figure 1A) (e.g., Cruden, 1977; Baecher and Lanney, 1978; Einstein and Baecher, 1983; LaPointe and Hudson, 1985; Pickering et al., 1995). Such joints are referred to as singly or doubly censored, respectively. If the censored portion of such data is ignored when estimating density or tracelength (Figure 1A-D), the estimated parameters will be incorrect. Density is overestimated due to censoring if the count of observed fractures is used as a proxy for the number of fracture centers. Mean tracelength is underestimated with visible traces because censoring hides portions of some traces (Figure 1D). The error decreases as the size of the sampling window increases relative to the length of the joints (Figure 1C). For example, in Figure 1A, the estimated mean tracelength of set 2 increases from 10.29 m for a circular window of radius 25 m to 17.12 m for a circular window of radius 75 m, which more closely approaches the true mean tracelength of 20.00 m.

Length bias occurs because longer joint traces having a greater probability of being sampled than shorter fracture traces (Baecher and Lanney, 1978; Einstein and Baecher, 1983; LaPointe and Hudson, 1985). Oversampling of longer traces causes the estimated tracelength distribution and estimates for mean tracelength to be positively skewed (Figure 1E).

Pattern heterogeneity is a change in joint characteristics, such as intensity, with a change in position. To prevent this effect from biasing estimates for joint characteristics, subregions within the pattern, with statistically homogeneous joint characteristics, are identified and sampled separately (LaPointe and Hudson, 1985; Ghosh and Daemen, 1993; Kulatilake et al, 1993b; Kulatilake et al., 1996; Kulatilake et al., 1997). If homogeneous subregions cannot be found, geostatistical methods may be employed to characterize the magnitude and rate of change as a function of distance and direction (LaPointe and Hudson, 1985; Priest, 1993; LaPointe, 1993; Jian et al., 1996). For this thesis, fracture pavements will be subdivided into homogeneous subregions based on visual inspection.

Advantages/Disadvantages of Current Estimation Methods

Straight scanlines (Figure 2) provide a rapid means for estimating fracture intensity and mean fracture tracelength (Priest and Hudson, 1981; LaPointe and Hudson, 1985; Becker and Gross, 1996). Straight scanlines, however, are subject to orientation bias, length bias, censoring, and the spatial heterogeneity of the fracture set (Terzaghi, 1965; Baecher and Lanney, 1978; Pahl, 1981; Priest and Hudson, 1981; Kulatilake and Wu, 1984a, b; LaPointe and Hudson, 1985; Priest, 1993; Wu and Pollard, 1995; Mauldon and Mauldon, 1997).

Areal sampling (Figure 2), which considers fracture traces over a two-dimensional region, is subject to orientation bias for anything except a circular sampling area, and reduces censoring and length bias as compared with a scanline sample. Because areal sampling averages trace parameters over an area, spatial heterogeneity is reduced (e.g., Wu and Pollard, 1995; Kulatilake et al., 1997). The effects of censoring and length bias are reduced as the size of the sampling region increases with respect to the length of the joint traces because most traces become completely visible. Drawbacks of the area method are that: (1) it is time consuming; (2) it may disguise spatial heterogeneities; and (3) inequant or small sampling areas such as those commonly available to the geologist reintroduce biases (LaPointe and Hudson, 1985; Kulatilake et al, 1993b; Wu and Pollard, 1995; Kulatilake et al., 1996). Thus, neither areal sampling nor straight scanlines are completely satisfactory in terms of efficiency and accuracy.

2. NEW FRACTURE ESTIMATORS

To combine the time efficiency of scanlines with the improved accuracy of areal sampling, this thesis examines a third approach that uses circular scanlines and circular windows (Figure 2) to estimate intensity, density and mean tracelength. An unbiased estimate of intensity is obtained from a count of the number of joint intersections with a circular scanline (Figure 3A) (Mecke, 1981; Stoyan et al., 1995; Mauldon et al., 1999a). An unbiased estimate of density is obtained from a count of the number of joint endpoints inside the circular window (Figure 3B) (Mauldon, 1998; Mauldon et al., 1999b). An asymptotically unbiased estimate of mean tracelength is obtained from the ratio of number of intersections on the circle to the number of endpoints inside the circle (Figure 3B) (Mauldon, 1998; Mauldon et al., 1999b).

The use of circular scanlines and windows combines the speed of straight scanlines with the bias reduction of areal measurements. The estimators are distribution-free, and do not require particular fracture spacing, tracelength or orientation distributions to estimate intensity, density or mean tracelength (Mauldon, 1998; Mauldon et al., 1999a, b).

Intensity

Previous workers have suggested the use of circular scanlines to eliminate orientation bias (Baecher and Lanney, 1978; Titley et al., 1986; Davis and Reynolds, 1996), but intensity estimators using circular scanlines have not been described previously in the geologic literature. Using principles of stochastic geometry, a circle-based intensity estimator for microscopy was described by Mecke (1981) and Stoyan et

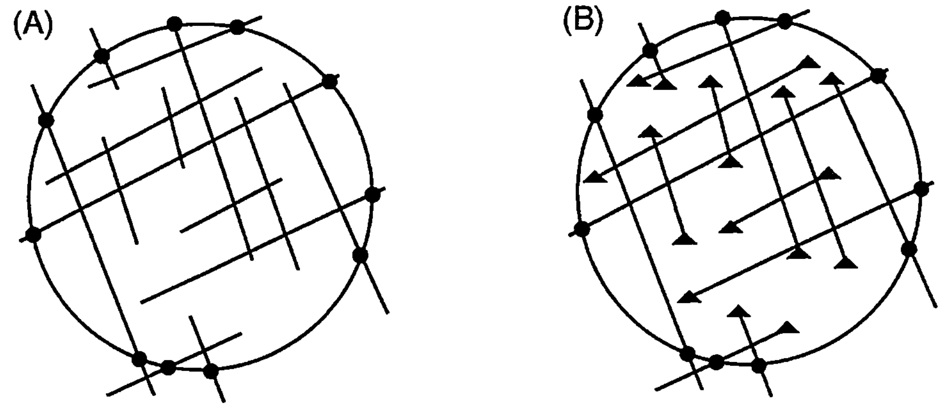

Figure 3 - Fracture pattern with circle illustrating n and m. (A) Solid dots represent the intersection points (n) between joints and circle. (B) Dots for the intersection points (n) of joints with the perimeter and triangles for joint endpoints (m) in a circular window

al. (1995) (see also Santaló, 1976). The intensity estimator, which was derived using a simplified analysis and applied to rock fractures by Mauldon et al. (1999a) is:

$$\hat{I} = n / 4r, \tag{1}$$

where $\hat{I}$ is the estimate of fracture intensity, n is the number of fractures intersecting the circumference of the circle (Figure 3A), and r is the radius of the circular scanline. For example in Figure 3a, n is 11, the circle radius is 1 m, and so the intensity estimate is 2.75 m^{-1}.

Density

To eliminate censoring and length bias when estimating the number of fracture centers in a sampling domain, Kulatilake and Wu (1984a) assumed a negative exponential tracelength distribution and determined the probability that the midpoint of a given fracture trace lies inside the window. A significant drawback of this method is that the tracelength distribution of a joint population is not generally known. Mauldon (1998) derived a distribution-free (Maritz, 1981) density estimator for sampling windows using the principle of associated points (Parker and Cowan, 1976), utilizing the two-to-one correspondence between trace endpoints and trace centers. The estimator simplifies for circular windows (Mauldon, 1998; Mauldon et al., 1999b):

$$\hat{\rho} = \frac{m}{2\pi r^2}, \tag{2}$$

where $\hat{\rho}$ is the estimate of fracture density, m is the number of fracture endpoints inside the circular window, and r is the radius of the circular window (Figure 3B). For example in Figure 3B, m is 17, the circle radius 1 m, and the estimate of density is 2.71 m^{-2}.

Mean Tracelength

Estimates of mean tracelength using straight scanlines or rectangular windows have been suggested (Cruden,1977; Baecher and Lanney,1978; Baecher,1980; Priest and Hudson,1981; Panek,1985; Rouleau and Gale,1985; Villaescusa and Brown,1992; Kulatilake et al., 1993b). These estimates of mean tracelength, however, assume underlying tracelength distributions, which are generally not known because the observed distributions themselves are subject to censoring and length bias. A quasi-distribution-free method of estimating mean fracture tracelength for traces with a fixed orientation, using a rectangular window, was introduced by Pahl (1981) and later modified by Kulatilake and Wu (1984b) to allow variable orientation. Mauldon (1998) derived a distribution-free estimator for mean fracture tracelength using an arbitrary convex window that is valid for any distribution of tracelength and trace orientation. The estimator simplifies for circular windows (Mauldon, 1998; Zhang and Einstein, 1998; Mauldon et al., 1999b):

$$\hat{\mu} = \frac{\pi r}{2}\left(\frac{n}{m}\right), \qquad (3)$$

where $\hat{\mu}$ is the estimate of mean fracture tracelength, r is the radius of the circular window, n is the number of fractures intersecting the circumference of the circular window (Figure 3B), and m is the number of fracture endpoints inside the circular window (Figure 3B). For example, in Figure 3B, *n* is 11, *m* is 17, the circle radius is 1 m, and so the estimated mean tracelength is 1.02 m.

3. DATA COLLECTION AND ANALYSIS

The performance of these new estimators is examined in this thesis via Monte Carlo simulation of synthetic fracture sets, and by application to natural fracture pavements from Llantwit Major and Amroth, Wales, UK; Tequesquite Creek (near Del Rio); Texas, USA; Rocky Creek (near Great Falls), South Carolina, USA; Telpyn Point (near Amroth), Wales, UK; Ward Lake (near Bishop), CA, USA; and P100, Yucca Mountain, NV, USA (Figures 4-10).

Synthetic Fracture Patterns

Synthetic fracture patterns were used to evaluate the fracture intensity, density and mean tracelength estimators, because all parameters for synthetic patterns can be controlled. Since all pertinent fracture parameters are known, the estimated values can be compared to the known values to evaluate the performance of the new estimators.

JAWS

Monte Carlo simulation (Hammersly and Handscomb, 1965) of fracture traces using JAWS (Joint Analysis using Windows and Scanlines, Appendices A and B), a Visual Basic® 5.0 computer program developed for this research, was used to evaluate the quality of the fracture intensity, density and mean tracelength estimators. In the program, synthetic sets of fracture traces, with centers generated from a Poisson distribution, were generated over a square generation region with an edge length of D + L (Figure 11). The estimators were evaluated over a smaller square analysis region (Gilmour et al., 1986)

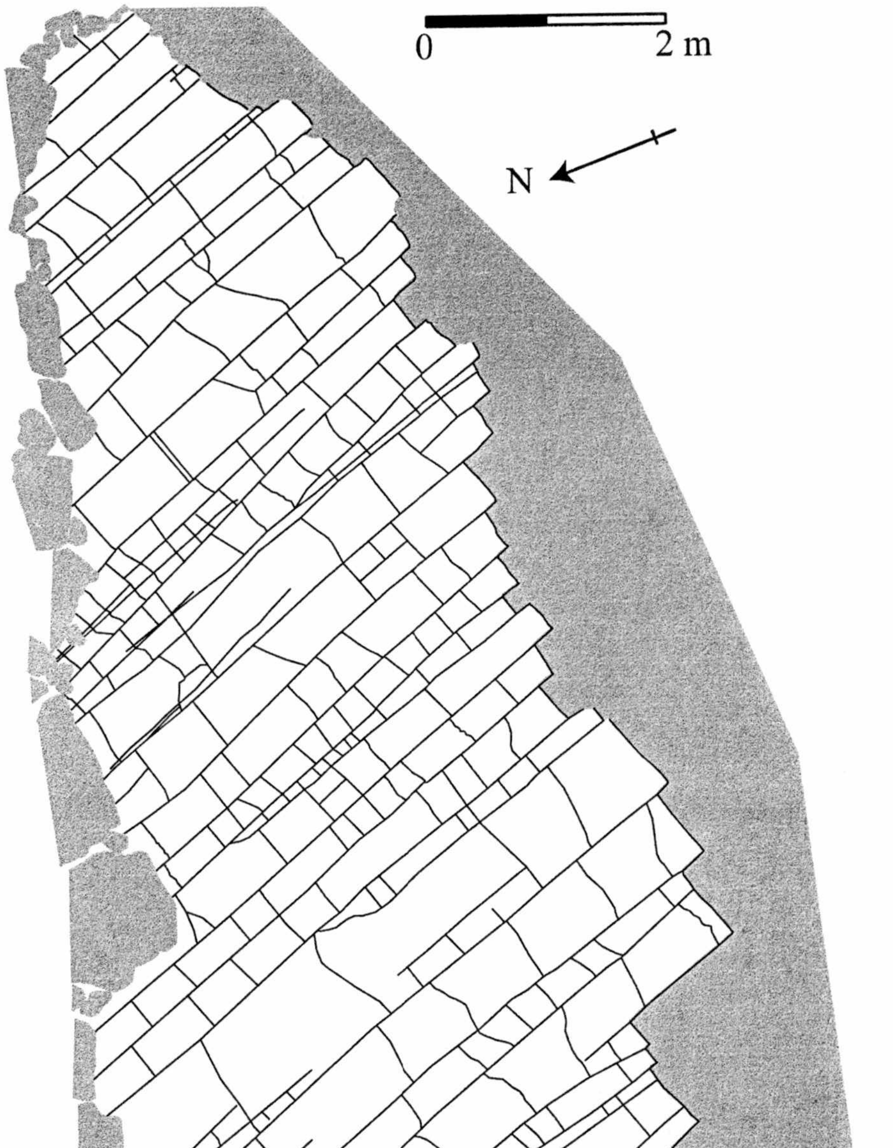

Figure 4 - Llantwit Major fracture trace map. Gray areas are covered or not mapped.

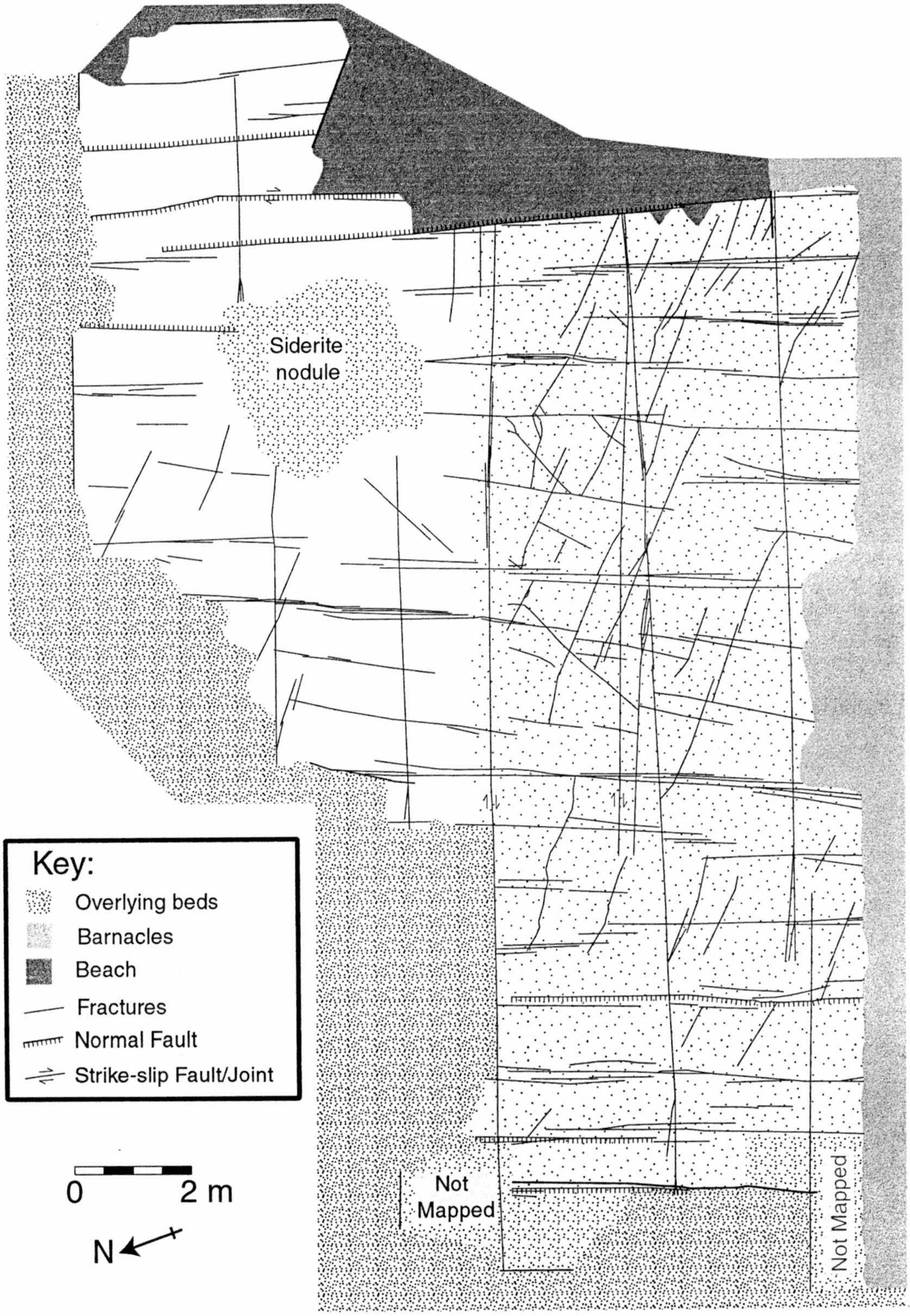

Figure 5 - Amroth fracture trace map. Lightly stippled region represents a homogeneous subdomain.

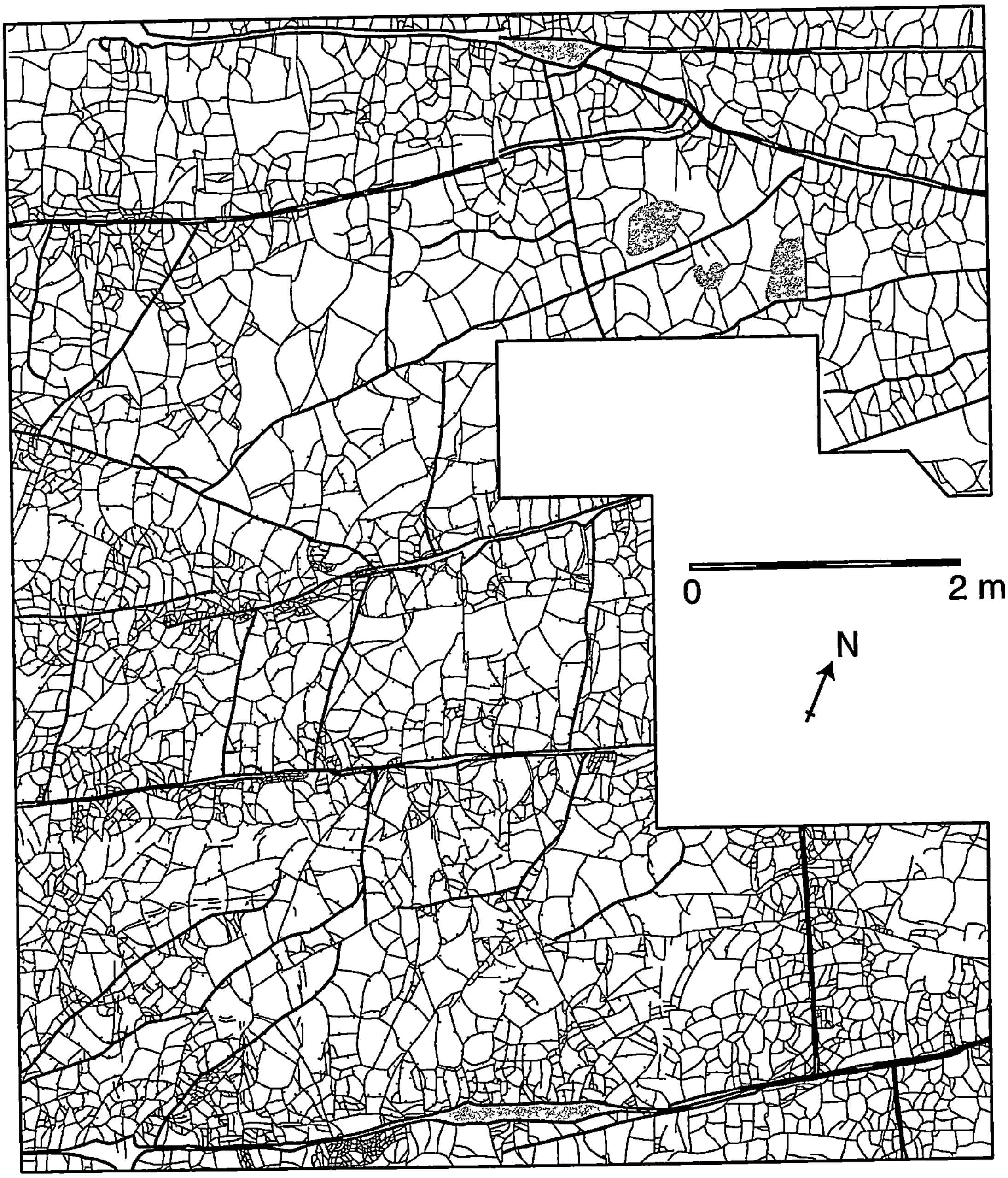

Figure 6 - Tequesquite Creek fracture trace map (modified from Wiltschko et al., 1991). Gray areas represent fossils or covered areas. Thick black joints were not analyzed. Lightly stippled region represents a homogeneous subdomain.

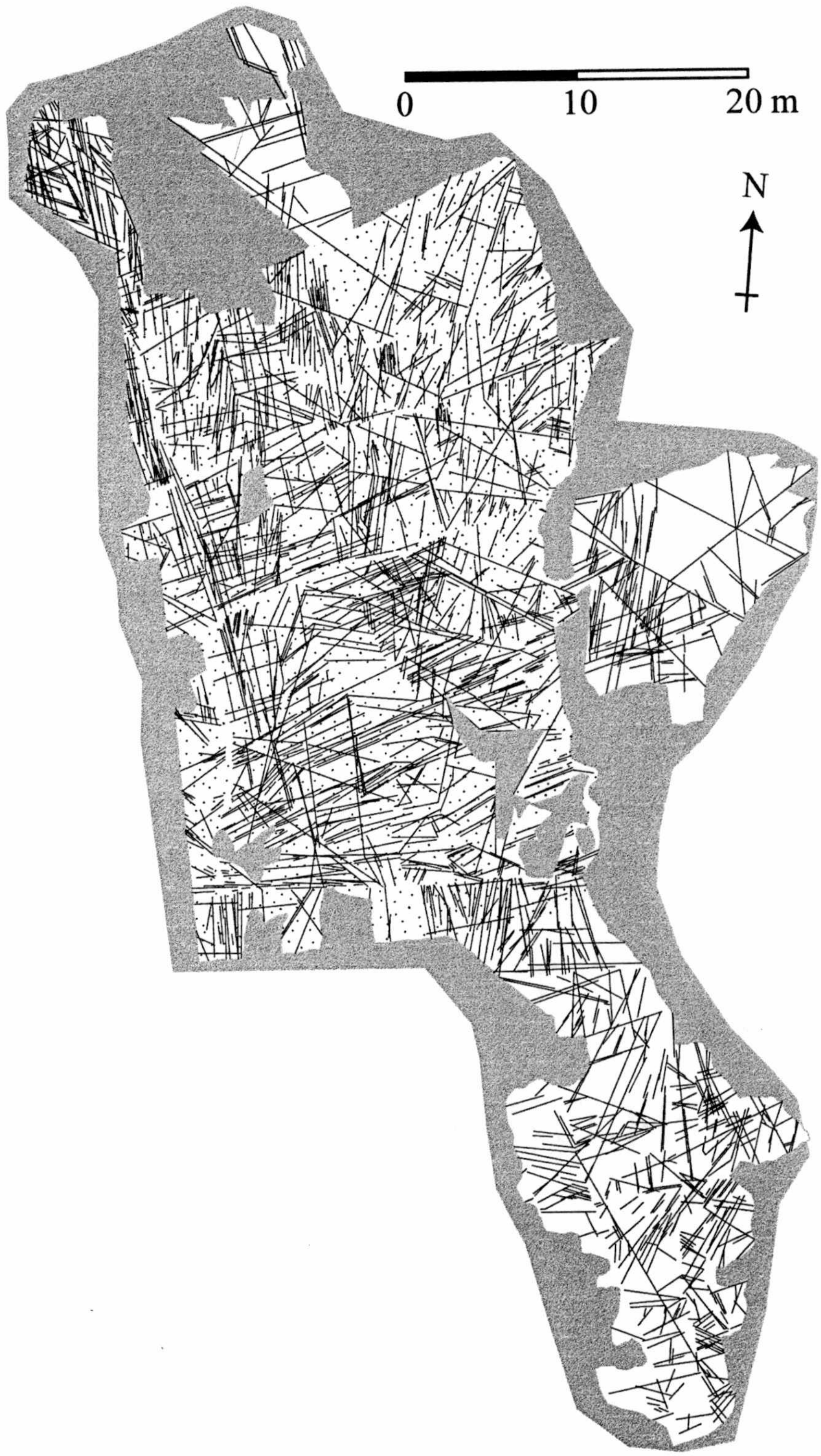

Figure 7 - Rocky Creek fracture trace map (modified from Schaeffer, 1998, unpublished data). Gray areas are covered or not mapped. Lightly stippled region represents a homogeneous subdomain.

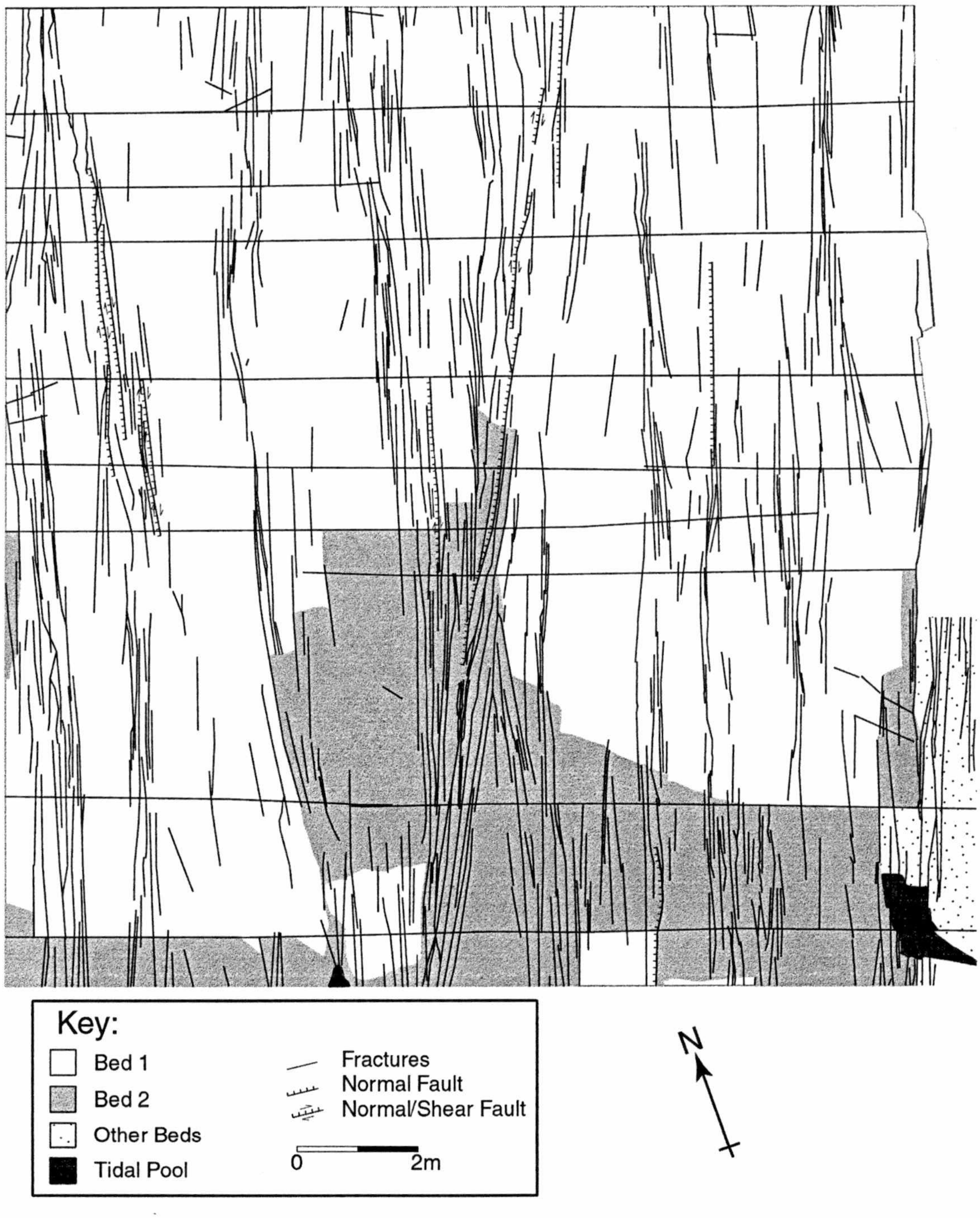

Figure 8 - Telpyn Point fracture trace map.

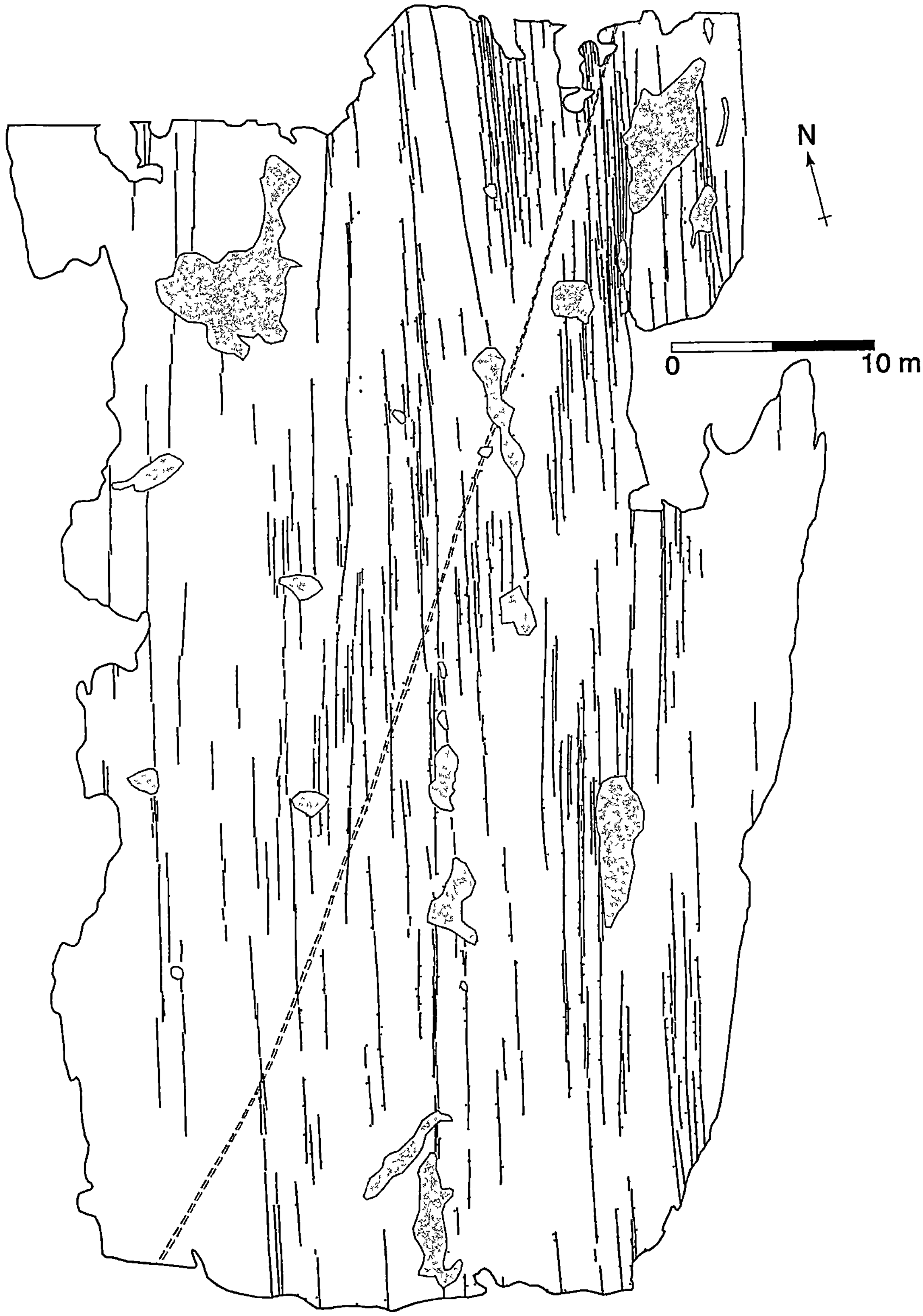

Figure 9 - Ward Lake fracture trace map (modified from Segall and Pollard, 1983). Gray areas are covered. Lightly stippled region represents portion of pavement analyzed. Pair of closely spaced, dashed lines show an aplite dike and was not analyzed.

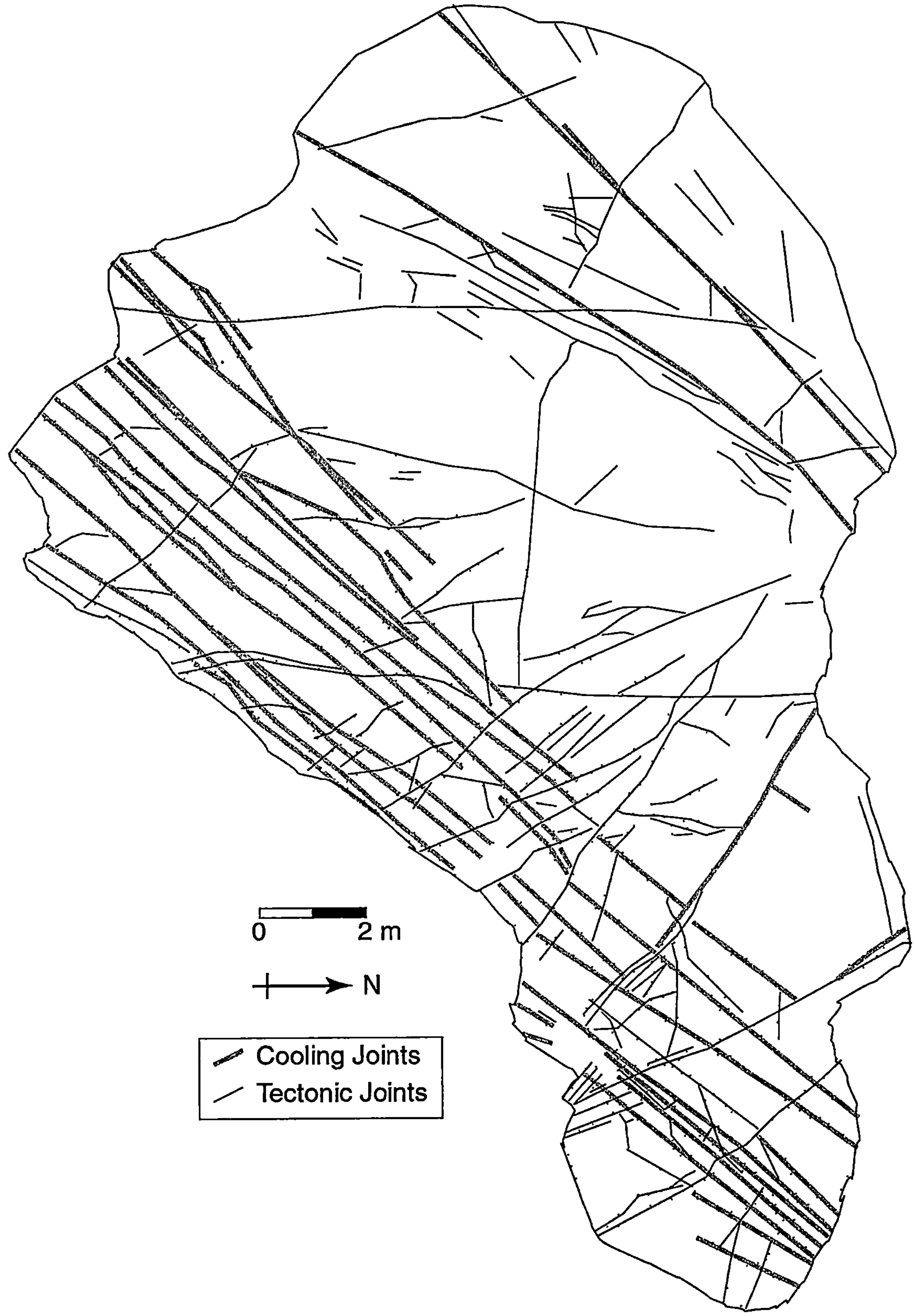

Figure 10 - P100 fracture trace map (modified from Barton et al., 1993). Lightly stippled region represents the portion of the pavement analyzed.

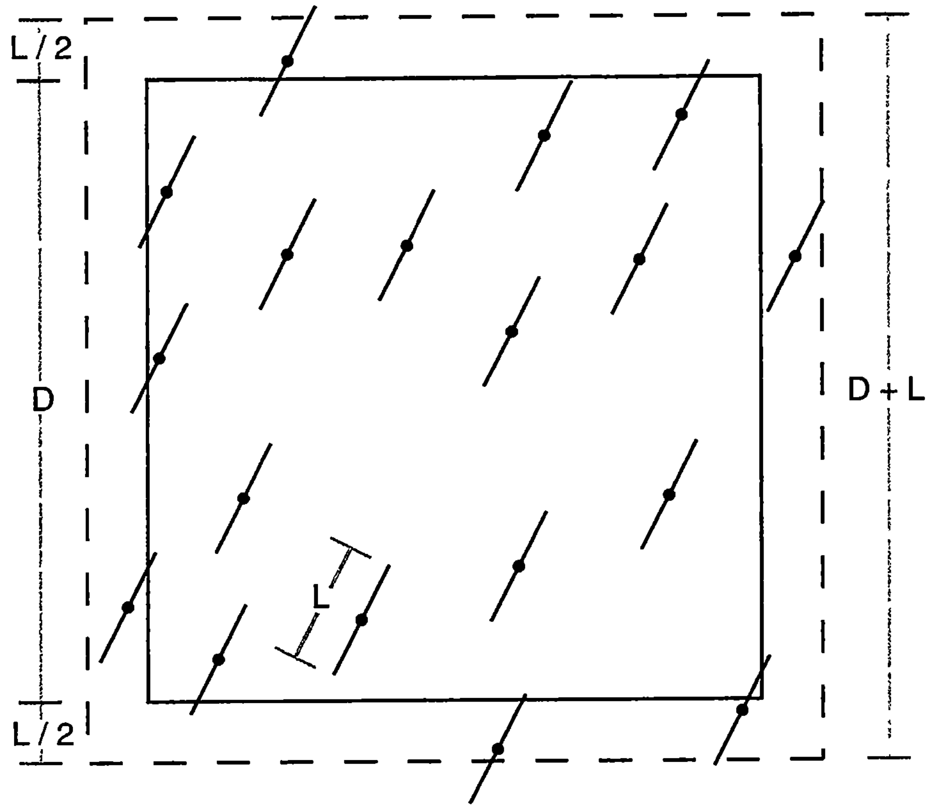

Figure 11 - Fracture centers (dots) and fractures (black lines) are generated in a generation region (dashed box) of size D + L, where L is the length of the longest fracture. The fractures are analyzed in the analysis region (box) of size D.

that was centered on the generation region and had an edge of length D, so as to avoid edge effects (Figure 11). The variables in these simulations were the density of fracture centers, mean tracelength, fracture orientation and the number and size of circular scanlines or windows used to sample these synthetic traces. Fracture intensity, which is not directly input, is a dependent variable because it is the product of density and mean tracelength.

Natural Fracture Patterns

The fracture patterns (Figures 4-10) formed in various geologic settings and lithologies, and represent a range of network geometries (Table 1). By applying the new estimators to this variety of natural fracture patterns, it was hoped to demonstrate the robustness of the new estimators for natural joint patterns. Only the trace maps shown in Figures 4-7 were used for initial analysis, but all fracture pavements were used to determine the 95% prediction interval for intensity estimates.

Data Analysis

A simple field procedure for gathering the new data sets would have been to use string, chalk and a measuring tape to establish circular scanlines and windows for the measurement of n and m. However, because the results needed to be compared to other methods fracture trace maps were constructed for the new field sites (Table 1).

New and existing maps were digitized and imported into JAWS where the patterns could be rapidly analyzed. After specifying the number and size of the circular

Table 1. Pavement Properties and Geology

Name, Location, Figure #	Rock Age and Formation Name	Source, Truncation Limit, Mapping Scale, Pavement Area	Joint Sets	Pattern Geometry	Origin
Llantwit Major, Wales, UK, SS95756754* (Figure 4)	Early Jurassic, Porthkerry Fm (limestone)	This study, 20 cm, 1 25, 49 5 m^2	cross – 075° master – 165°	ladder pattern with a bimodal trace length distribution	165° set formed during Late Cretaceous / Early Miocene Alpine compression (Nemcock et al , 1995) 075° set formed due to relaxation or contraction at later stage (Rawnsley et al , 1998)
Amroth, Wales, UK, SN17560722* (Figure 5)	Early Westphalian (Carboniferous), Early Westphalian coal measures (sandstone)	This study, 40 cm, 1 20, 162 0 m^2 (exposed area), 104 7 m^2 (stippled area)	200°, 290°, 316°	orthogonal pattern (200° & 290°), and one younger joint set	200° and 290° set formed during alternating σ_2 and σ_3 stress directions during Variscan thrusting (Dunne and North, 1990)
Tequesquite Creek, TX, USA, 3398161 8 m E** 3215760 0 m N** (Figure 6)	Cretaceous, Dessau Member of Austin Chalk	Wiltschko et al (1991), ~2 cm, 1 24, 52 2 m^2 (exposed area), 24 4 m^2 (stippled area)	050°, 330°, "random"	curvilinear fracture traces (random set) separated by long continuous fractures	050° set is parallel to the Balcones fault zone and is early, the "random" set formed by stretching of the chalk as fold plunge developed (Wiltschko et al , 1991)
Rocky Creek, SC, USA, 511215 3 m E** 3821843 5 m N** (Figure 7)	Cambrian, Great Falls Metagranite	Schaeffer, 1998, unpublished data, 25 cm, 1 120, 1446 6 m^2 (exposed area), 922 2 m^2 (exposed, stippled area)	068°, 274°, 292°, 356°	Multiple fracture sets, length distribution is independent of orientation	Joints are at high angles and of tectonic origin, greenschist facies minerals along the joints 300 Ma, the laumontite mineralization relates to Mesozoic rifting 150 to 200 Ma (Schaeffer, 1999, personal communication)
Telpyn Point, Wales, UK, SN18330731* (Figure 8)	Late Namurian (Carboniferous), Upper Sandstone Group	This study, 40 cm, 1 25, 247 6 m^2	200°, 267°, 290°, 318°	orthogonal pattern (200° & 290°), other younger sets	same as Amroth
Ward Lake, CA, USA, not specified (Figure 9)	Cretaceous, Mt Givens Granodiorite	Segall and Pollard (1983), ~100 cm, unknown, 1835 6 m^2 (exposed area), 1169 1 m^2 (exposed, stippled area)	010-020°	single set	Age of joints has been reported as either pre-Eocene or post-Pliocene (Segall and Pollard, 1983), joint sets are of regional extent
P100, Yucca Mt , NV, USA, 562051 8 ft E*** 763407 7 ft N*** (Figure 10)	Miocene, Tiva Canyon Tuff (upper lithophysal zone)	Barton et al (1993), 20 cm, 1 50, 233 2 m^2 (exposed area), 124 1 m^2 (stippled area)	cooling – 050°, 320° tectonic - 010°, 040°, 325°, 359°	orthogonal set of cooling joints with the 050° being dominant, poorly developed tectonic joints	Cooling joints formed first during thermoelastic relaxation from cooling, the tectonic joints post-date cooling joints, based on termination relationships, the 325° tectonic set is oldest, followed by 359° set, with 040° set youngest (Barton et al , 1993)

*British National Grid Reference System (Universal Transverse Mercator system)
**Universal Transverse Mercator system for USA
***5000 ft grid based on Nevada State Plane coordinates, Nevada State Plane projection

scanlines or windows to be used, JAWS uniformly distributed the center coordinates of sampling circles on a fracture pavement. Only circles that were completely contained within the fracture map were retained for the analysis (Stoyan et al., 1995).

4. RESULTS

Do Circles Defeat the Biases?

The performance of the new estimators was first investigated qualitatively by sampling known synthetic fracture patterns in a square analysis region of edged dimensions 100 L (Table 2) using 100 circles of radius 20 L. L is an arbitrary unit of length for which any standard unit of length can be substituted. The individual sample results and their running means were calculated for comparison with the known input values of the parameters (Figure 12).

To show that the new estimators are unaffected by orientation bias, a fracture pattern with joint orientations uniformly distributed over a 60° spread between 30° and 90° was analyzed (Table 2, O.B.). To show that that the estimators are unaffected by censoring, a fracture pattern with censored traces was analyzed (Table 2, C.B.). If the estimators do not defeat censoring, they should underestimate intensity, density and/or mean tracelength. To show that the intensity and mean tracelength estimators are unaffected by length bias, a fracture pattern consisting of two fracture sets was analyzed (Table 2, L.B.[1]). The two fracture sets have similar densities but different fracture intensities of (0.51 L^{-1} versus 1.0 L^{-1}) and mean tracelengths (50 L versus 100 L). To demonstrate qualitatively that the density estimator is unaffected by length bias, two more fracture sets of equal intensity, but differing densities and mean tracelengths were analyzed (Table 2, L.B.[2]). If the estimators do not defeat length bias, estimates should be skewed towards the value of the longer set for average intensity, density and mean tracelength.

Table 2. Input Values for Sampling Bias Detection*

	O. B	C. B.	L. B[1] (short)	L B.[1] (long)	L B.[1] (comp)	L B.[2] (short)	L. B[2] (long)	L B.[2] (comp)
Intensity (L^{-1})	1 01	0.986	0.51	1.00	0 75	2 05	2.01	2 03
Density (L^{-2})	0.051	0 025	0.010	0 011	0.011	0.039	0 020	0.030
Length (L)+	20 ± 10	40 ± 10	50 ± 10	100 ± 10	75	50 ± 10	100 ± 10	75
Orientation+	060 ± 30°	060 ± 30°	060 ± 30°	150 ± 30°	NA	060 ± 30°	150 ± 30°	NA

*O. B = Orientation Bias, C B. = Censoring Bias, L. B.[1] = Length Bias Results for Intensity and Mean Tracelength,
L B.[2] = Length Bias Results for Density, comp = composite

+Length and orientation ranges bound uniform distributions

Figure 12 - Calculated estimates (black lines) and running means (small open circles) for intensity, density and mean tracelength for synthetic patterns where sampling biases could be present. Dashed line and corresponding values represent the input values. (A) Orientation bias. (B) Censoring. (C) Length bias.

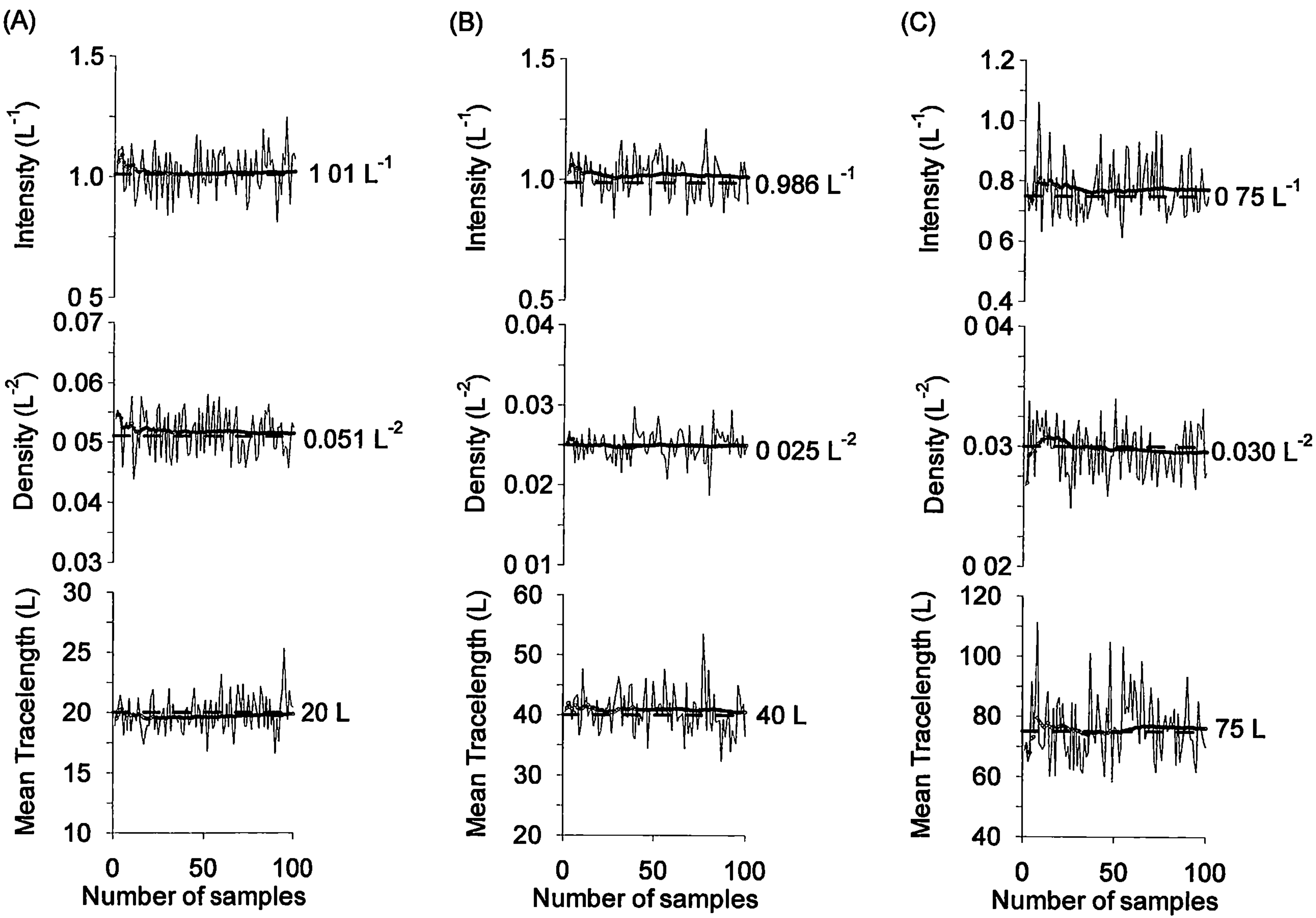
(A)
(B)
(C)
Intensity (L-1)
Density (L-2)
Mean Tracelength (L)
1 01 L-1
0.051 L-2
20 L
0.986 L-1
0 025 L-2
40 L
0 75 L-1
0.030 L-2
75 L
Number of samples

In all cases, the new estimators fluctuate about the input value, while the running means of the estimates approach the input values of the sample (Figure 12). So, on average, under- or overestimates are not produced, and the estimators are asymptotically unbiased with respect to orientation bias, censoring and length bias.

Comparison to Other Estimators

Having established that the new estimators overcome sampling biases, their performance was compared qualitatively to estimates from straight scanlines and areal sampling. A synthetic pattern (Figure 13) was generated for this comparison. Also, four natural patterns were used to compare to estimates from the area method, using the entire pavement as a single sample (Figures 4-7). The estimates using circular scanlines and windows were determined by averaging individual estimates from two to ten randomly positioned circles.

Fracture Intensity: Synthetic Fracture Patterns

A circular scanline radius of 10 L, an area sample equal to the circle area ($\approx$314 L^2), and a straight scanline of length equal to circle circumference ($\approx$63 L) were used for the comparison of the fracture intensity estimates. The circular scanline estimates of fracture intensity fluctuate about the input intensity, while their running mean approaches the input intensity as sample size increases (Figure 14A). Estimates from areal samples of the circular windows are almost identical to those for the circular scanlines. The time spent constructing a trace map to determine intensity is not efficient. To illustrate the

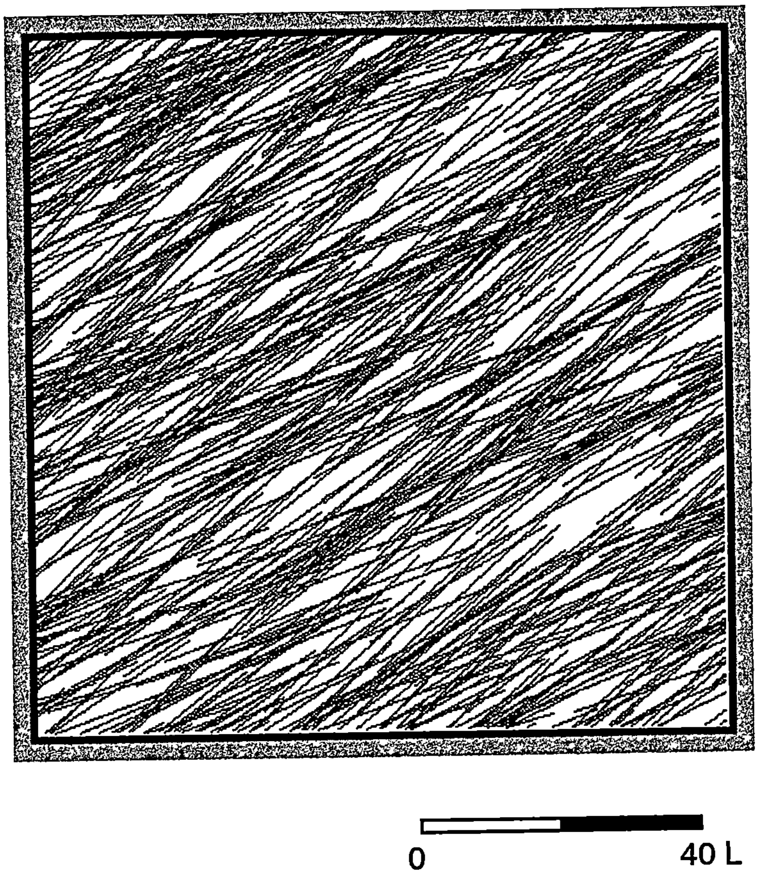

Figure 13 - Synthetic fracture pattern analyzed to test the new estimators versus existing estimators (input values: intensity = 2.0 L^{-1}, density = 0.05 L^{-2}, tracelength = 40 ± 20 L, orientation = 060° ± 30°). Pavement appears more intensely fractured, because the traces are artificially thick due to image resolution of 72 dpi. Orientation and length ranges bound uniform distributions.

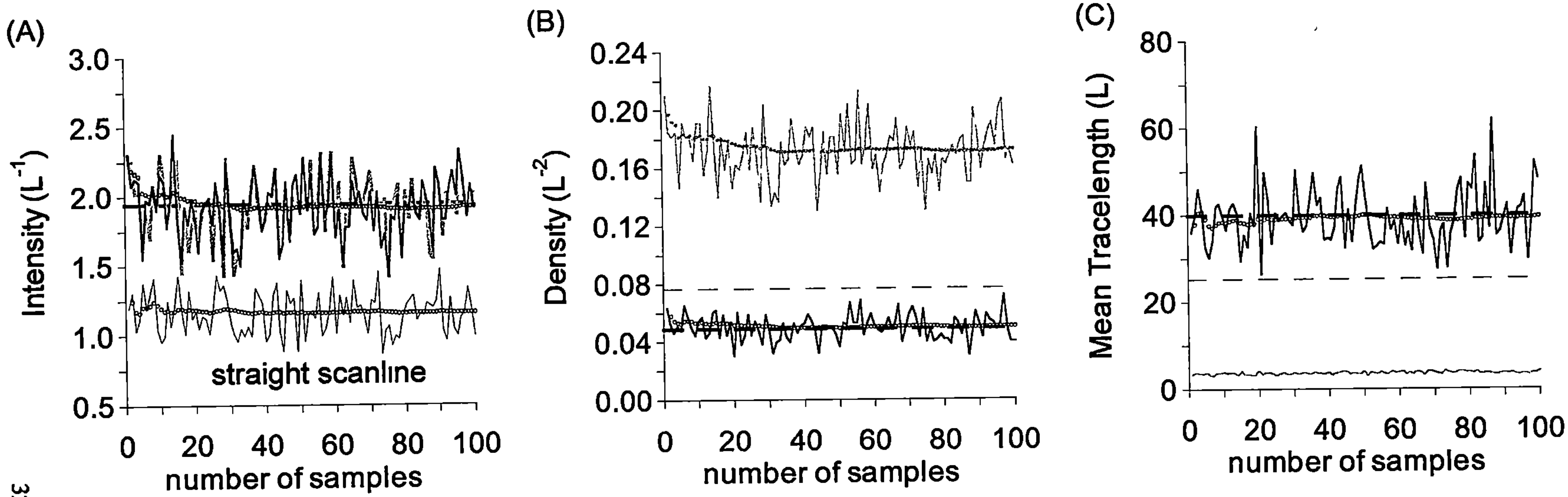

Figure 14 - Intensity, density and mean tracelength estimates using circular scanlines and/or windows, straight scanlines and areal sampling. (A) Estimates of intensity using circular scanlines (thick, black line), circular windows (light gray line), and straight scanlines (thin line). (B) Estimates of density using circular windows (thick, black line) and areal sampling of apparent density (light gray and dashed line). (C) Estimates of meantrace length using circular windows (thick, black line) and areal sampling of apparent tracelength (light gray and dashed line). Thick black, dashed lines are input values. Open circles are the running means.

orientation bias problem, a straight scanline oriented at 090° (E-W) was used to sample the pattern. Even though the data were corrected for orientation bias with a trigonometric correction applied to the mean set orientation (Terzaghi, 1965), intensity estimates still underestimated input intensity by a factor of 1.7.

Fracture Intensity: Natural Fracture Patterns

Generally, the variance of the new intensity estimator decreases with increasing circle radius at Llantwit Major, Amroth and Rocky Creek (Figure 15A, B, C, E). Circular scanlines do detect spatial heterogeneity in natural patterns, much like straight scanlines and unlike areal samples from the entire pavement (Wu and Pollard, 1995). At Llantwit Major, estimates for circular scanlines larger than $r = 1$ m slightly underestimate intensity as compared to the whole pavement. This effect occurs because large circles are restricted to the northwestern portion of the pavement where intensity is slightly lower (Figure 4, 15A, B). Similar heterogeneities are identified in the other three pavements, producing overestimates occur in these cases (Figure 15C-E). The overestimates occur for all circle sizes at Amroth, in a transition between $r = 1$ m and $r = 2$ m at Tequesquite Creek, and for circles of $r \geq 2$ m at Rocky Creek. In all cases, the estimates for circular scanlines and the sample from a pavement "window" become quite comparable when homogeneous subdomains are identified (stippled region, Figures 5-7). It should be noted that the circular scanlines also correctly estimate the intensities in the domains of the unstippled portions of the pavements.

Figure 15 - Intensity estimates from circular scanlines (diamonds) versus areal sampling (dashed line). (A) Master joints at Llantwit Major. (B) Cross joints at Llantwit Major. (C) All joints at Amroth. (D) All joints at Tequesquite Creek. (E) All joints at Rocky Creek. The numbers in parentheses give intensities, in m^{-1}, of the stippled portions of the pavement; numbers without parentheses give the intensities of the entire pavement.

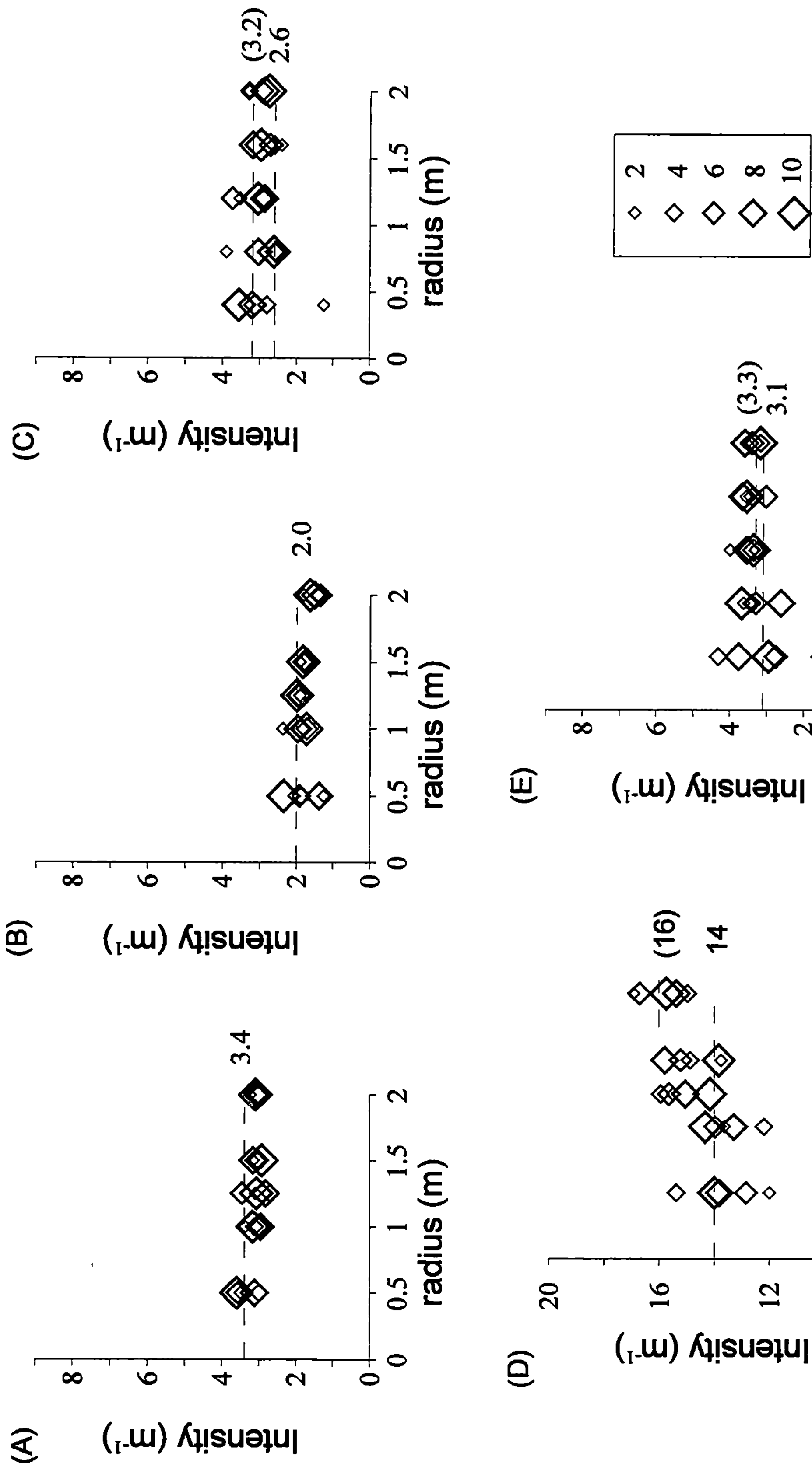
(A)
(B)
(C)
(D)
(E)
Intensity (m-1)
radius (m)
3.4
2.0
(3.2)
2.6
(16)
14
(3.3)
3.1
2
4
6
8
10

Fracture Density: Synthetic Fracture Patterns

Density estimates based on trace terminations in circular windows fluctuate about the input density and the running average approaches this density as the number of samples increases (Figure 14B). If the circular windows are treated as areas and the number of fractures in the window are counted, the apparent density overestimates the true density by a factor of 3.5 because of censoring and length bias. Increasing the size of the sample area (e.g., using the entire analysis square) reduces the overestimate (dashed line, Figure 14B) to a factor of 1.6, but nonetheless, counting all exposed pieces of fracture traces still generates a significant overestimate.

Fracture Density: Natural Fracture Patterns

Density estimates from circular windows at Llantwit Major, Amroth, Tequesquite Creek and Rocky Creek (Figure 16) are compared to the apparent density of the whole pavement. For natural patterns, the apparent density estimate from the entire pavement is closer to the unbiased density estimates from circular windows, especially at Rocky Creek (Figure 16E), than was the case for the synthetic example (Figure 14B vs. Figure 16). This difference occurs because the natural sample areas are mostly much larger in size, relatively, than the average length of the joints they contain as compared to the synthetic example (Figures 4-7 vs. 13). The clear exception is the master joint set at Llantwit Major (Figure 4, 16A) where almost all fractures are doubly censored. In this case, the apparent density overestimates by a factor of more than 3, as compared to the unbiased density estimates from the circular windows (1.5 vs. 0.35 m^{-2}). This significant

Figure 16 - Density estimates from circular windows (diamonds) versus areal sampling (dashed line). (A) Master joints at Llantwit Major. (B) Cross joints at Llantwit Major. (C) All joints at Amroth (D) All joints at Tequesquite Creek. (E) All joints at Rocky Creek. The numbers in parentheses give the apparent densities, in m^{-2},of the stippled portions of the pavement; numbers without parentheses give the apparent densities of the entire pavement.

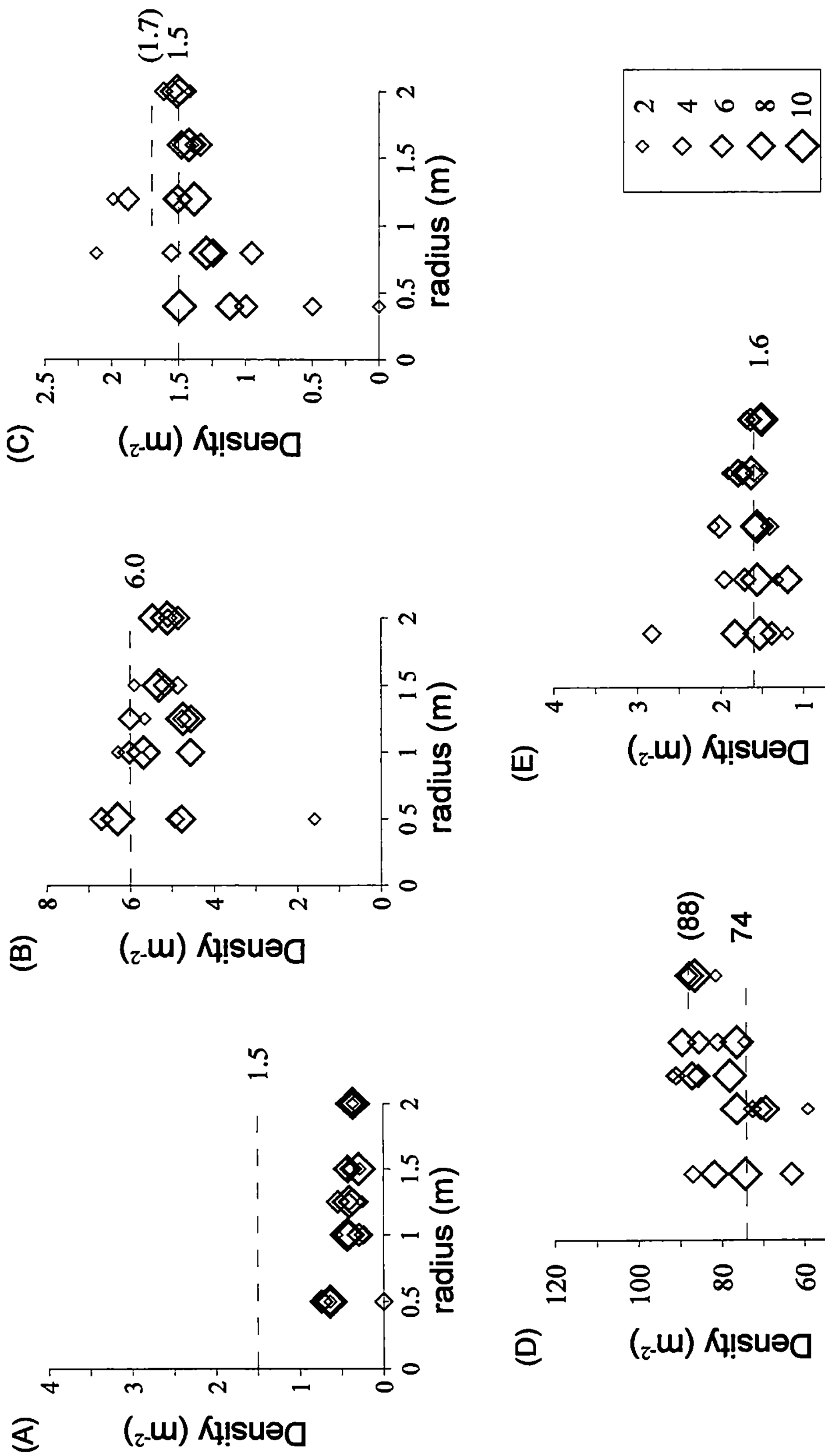

(A)
Density (m^{-2})
radius (m)
1.5
(B)
Density (m^{-2})
radius (m)
6.0
(C)
Density (m^{-2})
radius (m)
1.5
(1.7)
(D)
Density (m^{-2})
radius (m)
74
(88)
(E)
Density (m^{-2})
radius (m)
1.6
2
4
6
8
10

overestimate occurs because the dimensions of the pavement are small compared to the length of the fractures (i.e., the fractures are highly censored).

Significant changes in the estimates for windows with larger radii are again a function of spatial heterogeneity in the natural fracture patterns. As with the spatial variations in intensity, the larger circles are restricted to the same subdomains where density is also higher at Amroth and Tequesquite Creek. At Amroth the apparent density for the subdomain is still larger than the estimated density because the apparent values are censored.

Mean Fracture Tracelength: Synthetic Fracture Patterns

The circular window estimates of mean tracelength fluctuate about the input mean tracelength and the running average approaches this input value as the number of samples increases (Figure 14C). If the circular windows are treated as area samples and observed lengths are averaged, the measured tracelength yields a significant underestimate (i.e., a factor of 11) because of censoring. Increasing sample area size to the whole square analysis window decreases the magnitude of the underestimate (dashed line, Figure 14C) to a factor of 1.6. Nonetheless, censoring of traces is still a significant issue.

Mean Fracture Tracelength: Natural Fracture Patterns

The mean tracelength estimates from circular windows at Llantwit Major, Amroth, Tequesquite Creek and Rocky Creek (Figure 17) are compared to mean tracelength as determined for the whole pavements. Average estimates using multiple

Figure 17 - Tracelength estimates using circular windows (diamonds) versus areal sampling. (A) Master joints at Llantwit Major. (B) Cross joints at Llantwit Major. (C) 290° set at Amroth. (D) 200° set at Amroth. (E) 316° set at Amroth. (F) All joints at Tequesquite Creek. (G) All joints at Rocky Creek.

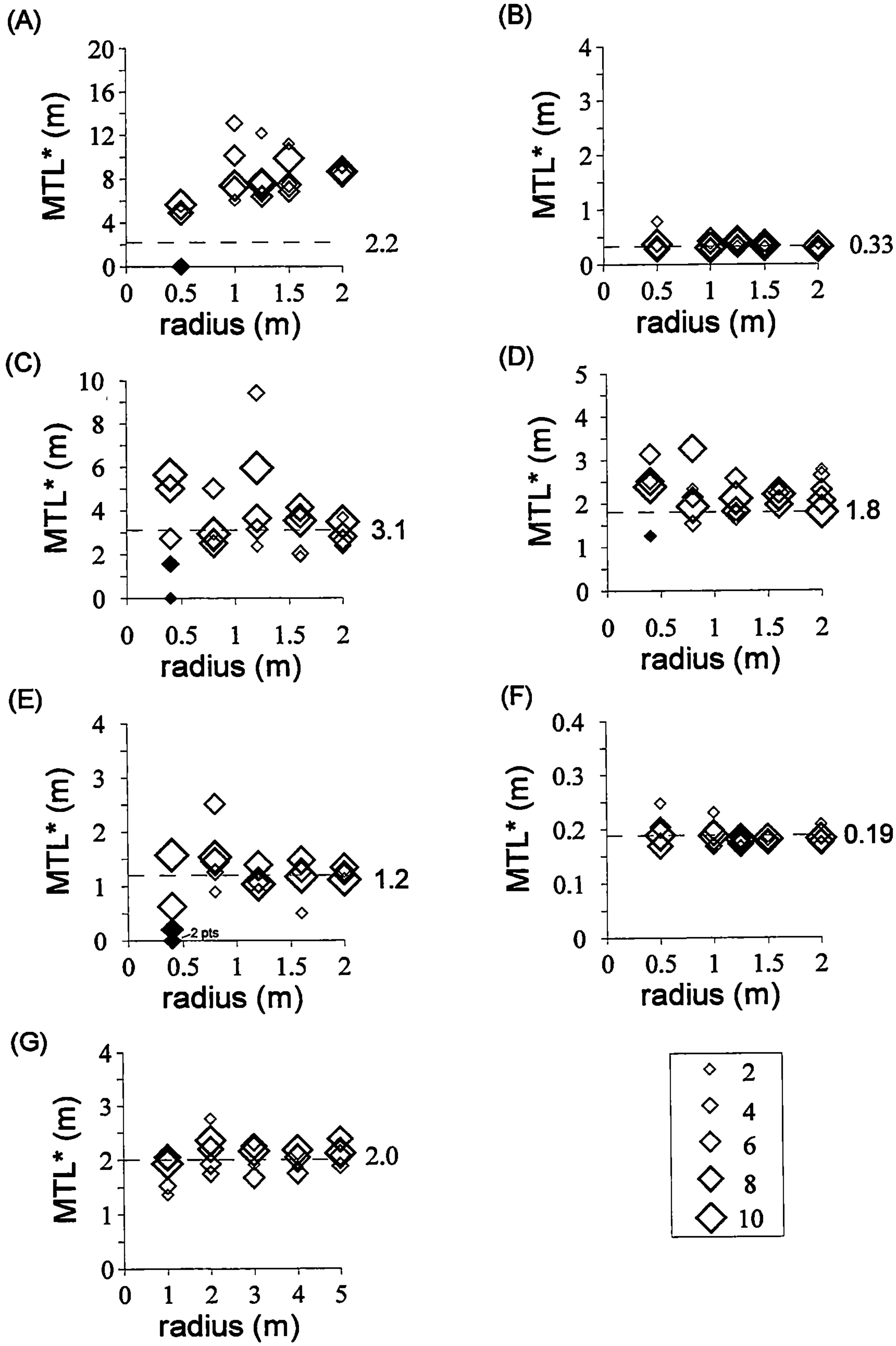

MTL* = Mean Tracelength

circles (for example, 10 circles) are calculated using

$$\hat{\mu} = \left(\frac{\overline{n}}{\overline{m}}\right)\frac{\pi r}{2}, \tag{4}$$

where $\overline{n}$ is the average number of intersections and $\overline{m}$ is the average number of endpoints, instead of

$$\hat{\mu} = \left(\overline{n/m}\right)\frac{\pi r}{2}, \tag{5}$$

as suggested by Zhang and Einstein (1998). By using equation 4, instead of equation 5, the effect of an individual mean tracelength estimate being infinity (i.e., $m = 0$) is reduced. For plotting points with zero $\overline{m}$ in equation 4, a nonzero value of 1 was substituted to allow the data point to be plotted. Such estimates are shown as solid diamonds and represent a lower bound for the estimator (Figure 17). The mathematical basis for the choice of equation 4 over equation 5 is given in Mauldon et al. (in review).

For the natural patterns, the apparent mean tracelength obtained from the entire pavement is comparable to the true mean tracelength estimates from circular windows, especially for the cross joints at Llantwit Major, 316° set at Amroth, and all joints at Rocky Creek and Tequesquite Creek (Figure 17B, E-G), than is the case for the synthetic example (Figure 14C). Again, this relationship exists because the natural exposures are mostly much larger relative to the average length of the joints as compared to the synthetic examples (Figures 4-7 vs. 13). The clear exception is the master joint set at Llantwit Major, which are mostly doubly censored and hence, should yield the worst estimates from the apparent tracelength (Figure 17A). Sampling the entire pavement, yields an apparent measure of 2.2 m, whereas circles with $r = 2$ m yield a tracelength estimate of 8.7 m, which, based on field observations (Figure 18), is closer to the true tracelength. In contrast, the degree of censoring for the 200° set at Amroth (Figures 5, 17D) is less than for the master joints at Llantwit Major, and hence the estimated mean tracelength is relatively close to the apparent mean. The 290° set at Amroth yields estimates that have a high degree of variability and center on the apparent mean tracelength of 3.1 m (Figure 17C). This variability occurs because visible tracelengths cover a large spectrum of values while the median is only 1.6 m (Figure 19). Long fractures skew the tracelength estimates such that the true mean tracelength happens to be approximately equal to the apparent mean tracelength in this case.

Summary

The new circular scanlines and window estimators successfully handle sampling biases, which plague the straight scanline and area methods (Figure 12). When applied to synthetic and natural patterns, the estimates of intensity, density and mean tracelength are representative of the population values (Figures 14-17) and for the cases of density and mean tracelength perform more accurately than the estimates using areal sampling. Accuracy of the estimates improves (i.e., variance decreases) as the sample size increases (Figures 15-17). These estimators are also extremely time efficient because they only require knowledge of n and m, as opposed to constructing a full trace map.

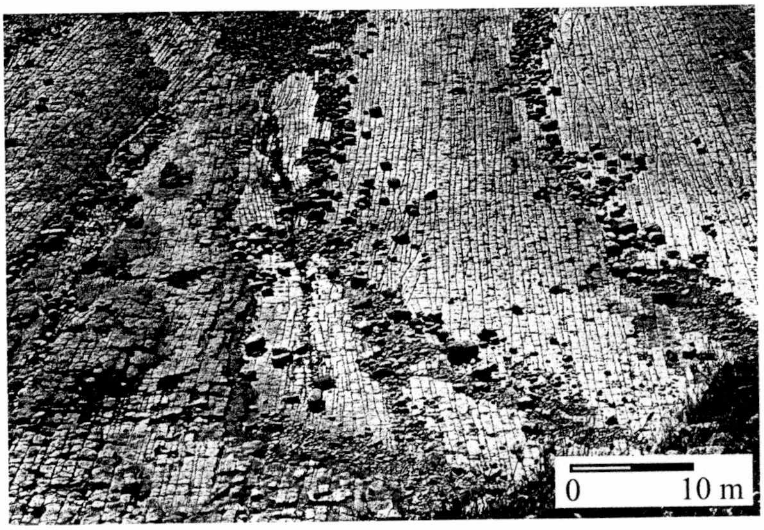

Figure 18 - Oblique aerial view of Llantwit Major site illustrating the length of the master joints (roughly vertical in figure).

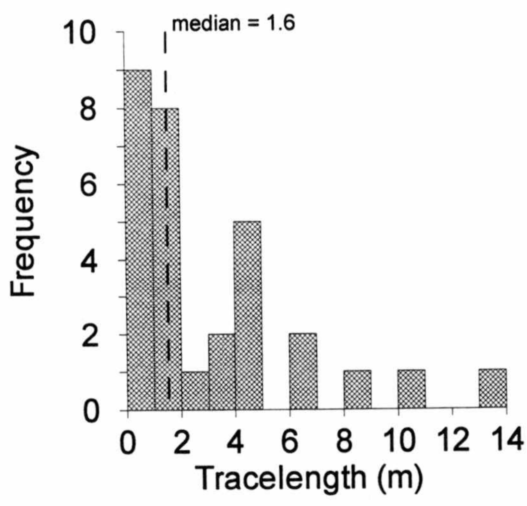

Figure 19 - Frequency plot of 30 visible tracelengths for the 290° set at Amroth.

Quantitative Analysis

A remaining issue is determining the confidence in the estimators. Previous approaches to determining the level of confidence in fracture sampling results include determining relative error versus scanline length for exponentially and lognormally distributed fracture spacings (Sen and Kazi, 1984), confidence bands for tracelength estimates using straight scanlines where the mean tracelength distribution is known (Zhang and Liao, 1990), confidence intervals for fracture spacing from straight scanlines (Priest, 1993), comparison of average fracture spacing (AFS) predictions from vertical wells to measured spacings in near-horizontal wells (Narr, 1996), distribution-dependent confidence intervals for mean tracelength estimates using areal samples (Pahl, 1981), and estimating the minimum sample size to be within 10% of the assumed value for area samples (Wu and Pollard, 1995). These approaches were not used because they require a large length (Narr, 1996) or number of samples (Priest, 1993), or distribution-dependent characteristics that may not be validated from existing data sets of natural fractures (Sen and Kazi, 1984; Zhang and Liao, 1990; Pahl, 1981).

The approach taken here is to determine the degree of confidence in predictions that would be made from a small number of estimates (i.e., 10 or less). This degree of confidence is determined by calculating the 95% prediction interval (PI) for distribution-independent estimates of characteristics such as intensity, density, or tracelength. The procedure identifies an interval on a graph (Figures 20A, B, 21A, B, 22A, B) where, on average, 95% of future estimates of that characteristic should fall for a particular sampling scheme (Bowerman and O'Connell, 1990; Hocking, 1996). To determine the

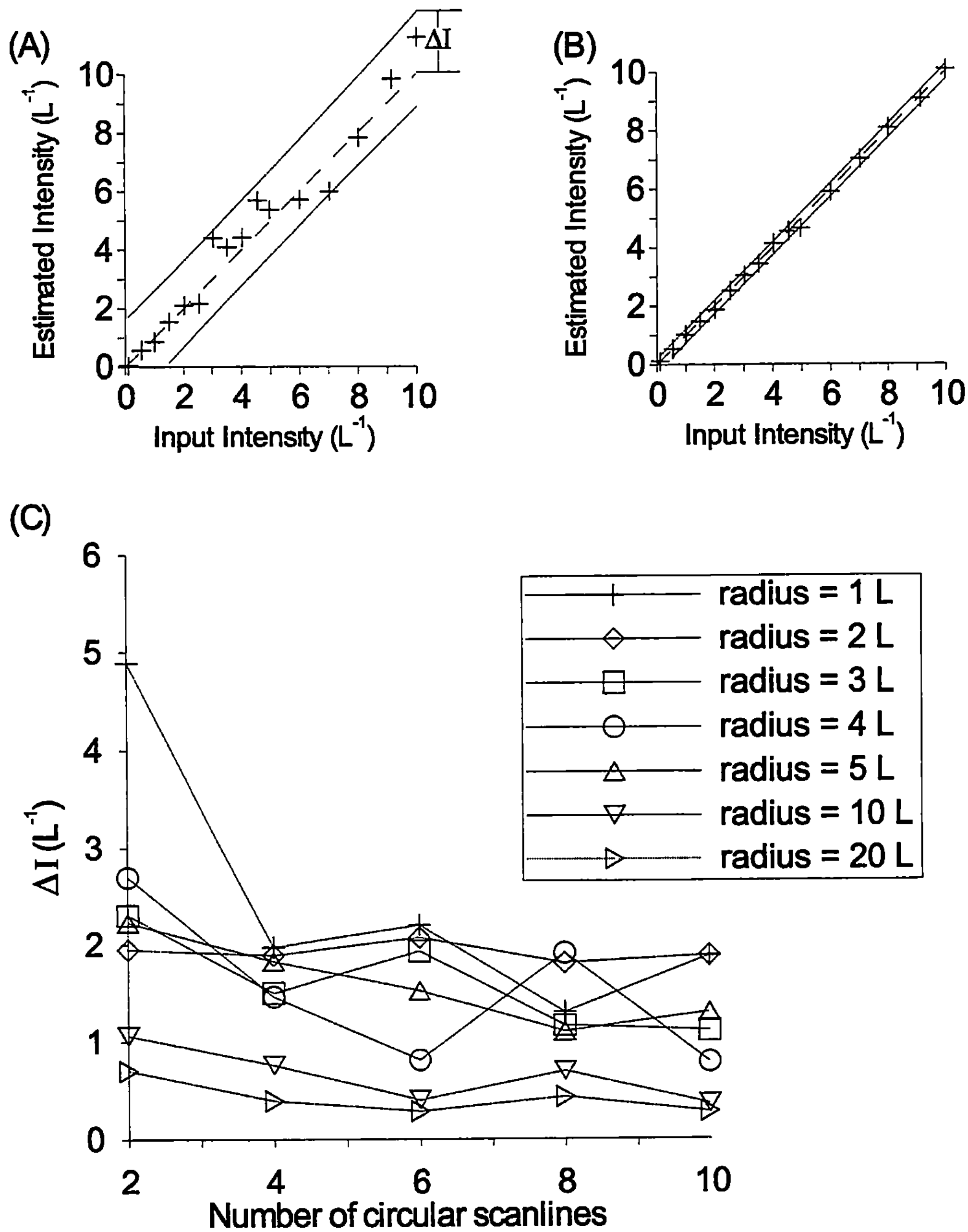

Figure 20 - Prediction interval data for intensity estimates from synthetic patterns. (A) 95% PI plot for average intensity estimates (plus signs) from 6 circles of radius 2 L. (B) 95% PI plot for average intensity estimates (plus signs) from 10 circles of radius 20 L. (C) Plot of ΔI (maximum error in intensity estimate) for 7 radii and 5 numbers of circles used to generate 35 sampling schemes for synthetic fracture traces. Dashed lines in (A) and (B) represents a perfect prediction; black lines in (A) and (B) represent upper and lower 95% PI. See Table 3 for input data.

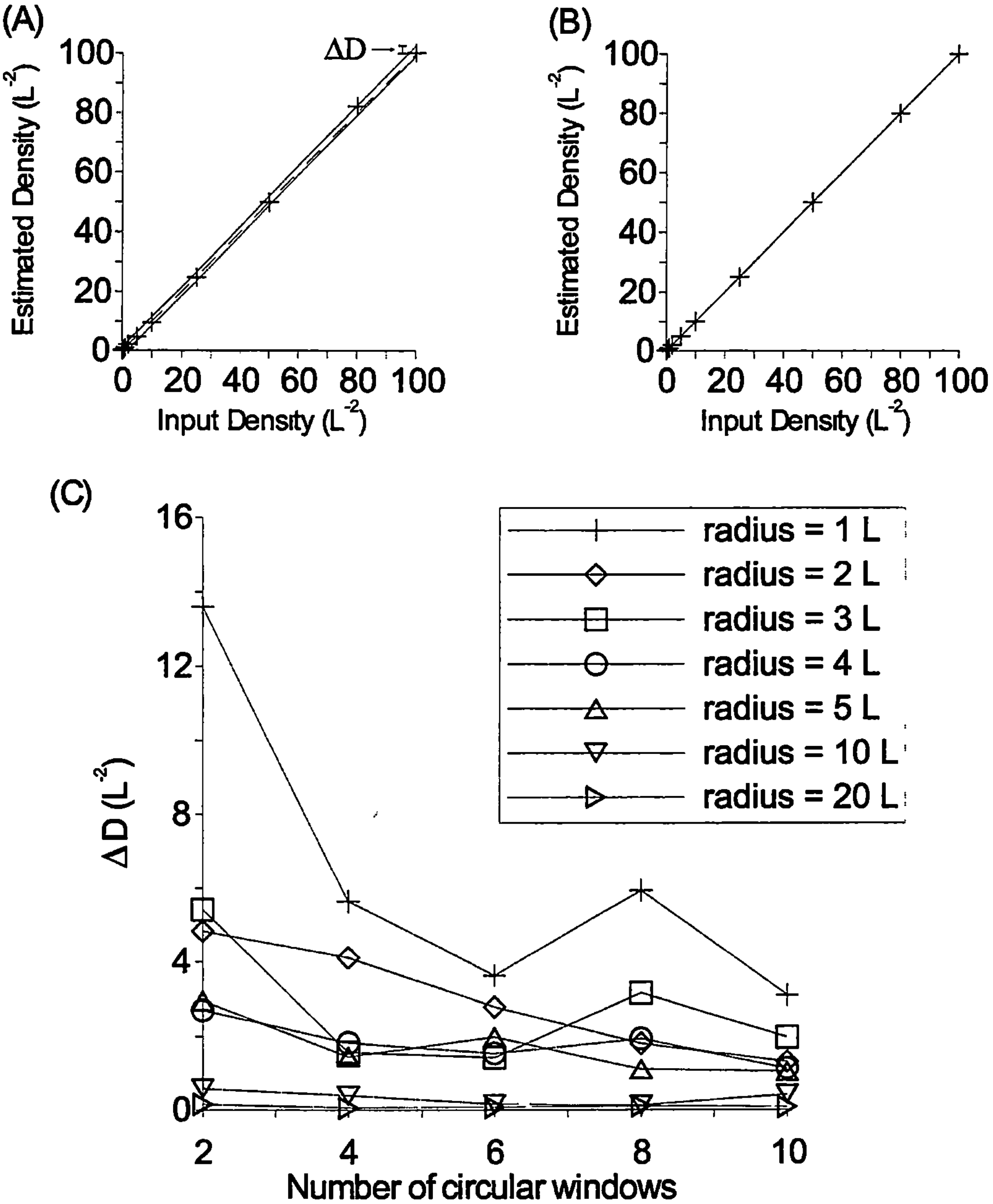

Figure 21 - Prediction interval data for density estimates from synthetic patterns. (A) 95% PI plot for average density estimates (plus signs) from 6 circles of radius 2 L. (B) 95% PI plot for average density estimates (plus signs) from 10 circles of radius 20 L. (C) Plot of ΔD (maximum error density estimate) for 7 radii and 5 number of circles used to generate 35 sampling schemes for synthetic fracture traces. Dashed lines in (A) and (B) represents a perfect prediction; black lines in (A) and (B) represent upper and lower 95% PI. See Table 4 for input data.

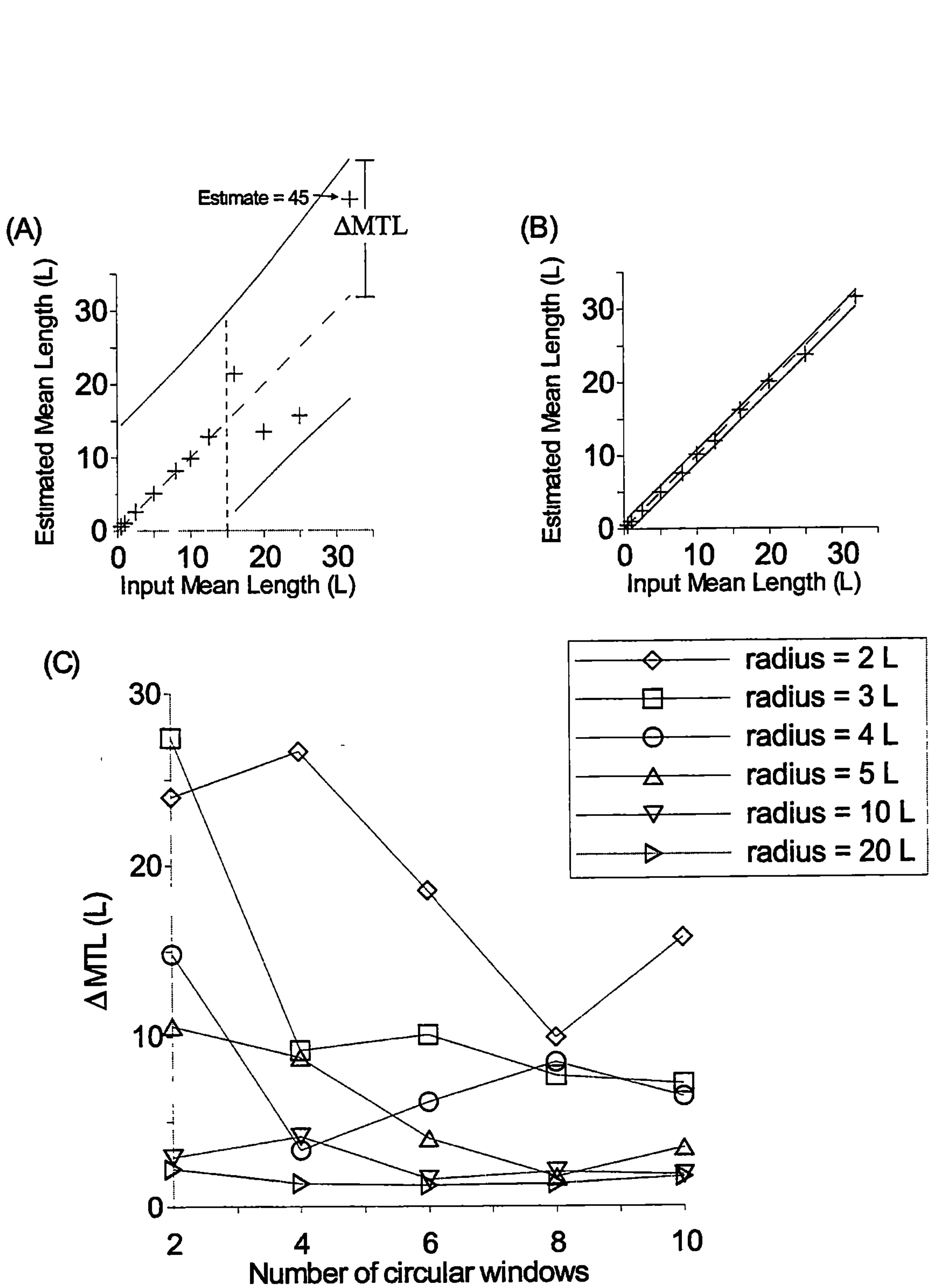

Figure 22 - Prediction interval data for mean tracelength estimates from synthetic patterns. (A) 95% PI plot for average mean tracelength estimates (plus signs) from 6 circles of radius 2 L. (B) 95% PI plot for average mean tracelength estimates (plus signs) from 10 circles of radius 20 L. (C) Plot of ΔMTL (maximum error between the perfect prediction and the 95% PI) for 6 radii and 5 number of circles used to generate 30 sampling schemes for synthetic fracture traces. Dashed lines in (A) and (B) represents a perfect prediction; black lines in (A) and (B) represent upper and lower 95% PI. See Table 5 for input data.

95% PI, a least-squares model for the data was chosen because estimated versus known values approximately plot on a 45° line. SAS 7.0®, a statistical software package, was used to calculate the 95% PI.

Synthetic Fracture Patterns

To determine the 95% PI for fracture intensity, density and mean tracelength estimates from different sampling schemes, fracture intensities ranging over two orders of magnitude from 0.1 to 10 L^{-1} (Table 3), densities ranging over three orders of magnitude from 0.1 to 100 L^{-2} (Table 4), and mean tracelengths ranging over nearly 2 orders of magnitude from 0.5 to 32 L (Table 5) were analyzed using the same 35 schemes. A sampling scheme is a particular combination of circle number and radius. Figures 20A, B, 21A, B and 22A, B show 95% PI plots for different sampling schemes. Each plot has a data point for the average estimate of intensity, density or mean tracelength as calculated for each sampling scheme. The maximum error, ΔI, ΔD or ΔMTL, between the perfect prediction (dashed lines, Figures 20A, B, 21A, B, 22A, B) and the 95% PI (solid lines) was determined for each sampling scheme. Since ΔI and ΔD are conservative measures and approximately constant over the range of values for a given sampling scheme (Figures 20A, B, 21A, B), ΔI and ΔD values were summarized for the 35 tested schemes (Figures 20C, 21C). Only 30 schemes were summarized for ΔMTL (Figure 22C) because the 95% PI could not be used to quantify estimates from a circular window of radius 1 L. This situation occurs because some of the mean tracelength estimates for traces longer than 20 L were infinity (i.e., $m = 0$ in equation 3). Unlike

Table 3. Input Data for Intensity Prediction Intervals

Intensity (L^{-1})	Density (L^{-2})	Tracelength (L)
0.11	0.003	40 ± 20
0 56	0 013	40 ± 20
1 0	0.025	40 ± 20
1 5	0 038	40 ± 20
2 0	0.050	40 ± 20
2.6	0 063	40 ± 20
3.0	0.075	40 ± 20
3.5	0 088	40 ± 20
4.0	0.10	40 ± 20
4 6	0.11	40 ± 20
5.0	0.13	40 ± 20
6.0	0.15	40 ± 20
7 0	0.18	40 ± 20
8 0	0 20	40 ± 20
9.2	0 23	40 ± 20
10	0 25	40 ± 20

Table 4. Input Data for Density Prediction Intervals

Density (L^{-2})	Intensity (L^{-1})	Tracelength (L)
0.1	2.0	20 ± 10
0.5	2.0	4 ± 2
1	2.0	2 ± 1
2	2 0	1 ± 0.5
5	2.0	0.4 ± 0.2
10	2.0	0.2 ± 0.1
25	2.0	0 08 ± 0.04
50	2 0	0 04 ± 0.02
80	2.0	0.025 ± 0.0125
100	2.0	0.02 ± 0 01

Table 5. Input Data for Mean Tracelength Prediction Intervals

Tracelength (L)	Intensity (L^{-1})	Density (L^{-2})
0.5 ± 0.25	2 0	4.00
1 ± 0.5	2.0	2.00
2.5 ± 1.25	2.0	0.80
5 ± 2.5	2 0	0.40
8 ± 4 0	2 0	0 25
10 ± 5.0	2 0	0.20
12 5 ± 6 25	2.0	0 16
16 ± 8 0	2.0	0 12
20 ± 10.0	2 0	0 10
25 ± 12.5	2 0	0 08
32 ± 16.0	2 0	0.06

Figures 20C, 21C and 22C, which show absolute magnitudes of error, Figure 23 plots the delta values as percent error and shows a substantial reduction in percent error with increasing intensity, density or mean tracelength.

Figures 20C, 21C and 22C suggest that greater quality is achieved by increasing circle radius rather than circle number. The increase in quality with larger circles occurs because the effects of pattern heterogeneity are averaged out. Although the fracture pattern is statistically homogenous for the sample window, the use of a Poisson process for trace centers allows spatial heterogeneity at the subwindow scale. A measure of this pattern heterogeneity is determined by considering the endpoints of the synthetic joints rather than their traces. Visualization of the spatial distribution in terms of endpoints is particularly appropriate because the number of endpoints (m) is a key parameter for the density and mean tracelength estimators. The spatial heterogeneity of points distributed in an area can be evaluated via a clustering test (Davis, 1986). A homogeneous pattern is anticlustered, whereas a spatially heterogeneous pattern exhibits clustering. The degree of clustering is determined by comparing the mean number of endpoints per subwindow to the variance of those endpoints.

For example, for an intensity of 2.0 L^{-1} and a density of 0.1 L^{-2}, the clustering test applied to trace endpoints in a grid containing 400 cells of size 5 L by 5 L showed that the fractures are clustered because the variance (3.8) is larger than the mean number of fracture endpoints (3.4). Clustering was also found for a larger sampling grid of 10 L by 10 L (variance = 16; mean = 14). For a grid of 20 L by 20 L, on the other hand, the variance (44) of m is less than the mean (54), and thus at the scale of this larger sampling

Figure 23 - Percent error plots for average intensity, density and mean tracelength estimates. (A) Intensity estimates from 6 circles. (B) Intensity estimates from 10 circles. (C) Density estimates from 6 circles. (D) Density estimates from 10 circles. (E) Tracelengths estimates from 6 circles. (F) Tracelength estimates from 10 circles. Long dashes for a radius of 2 L, solid line for a radius of 4 L, and short dashed for a radius of 10 L.

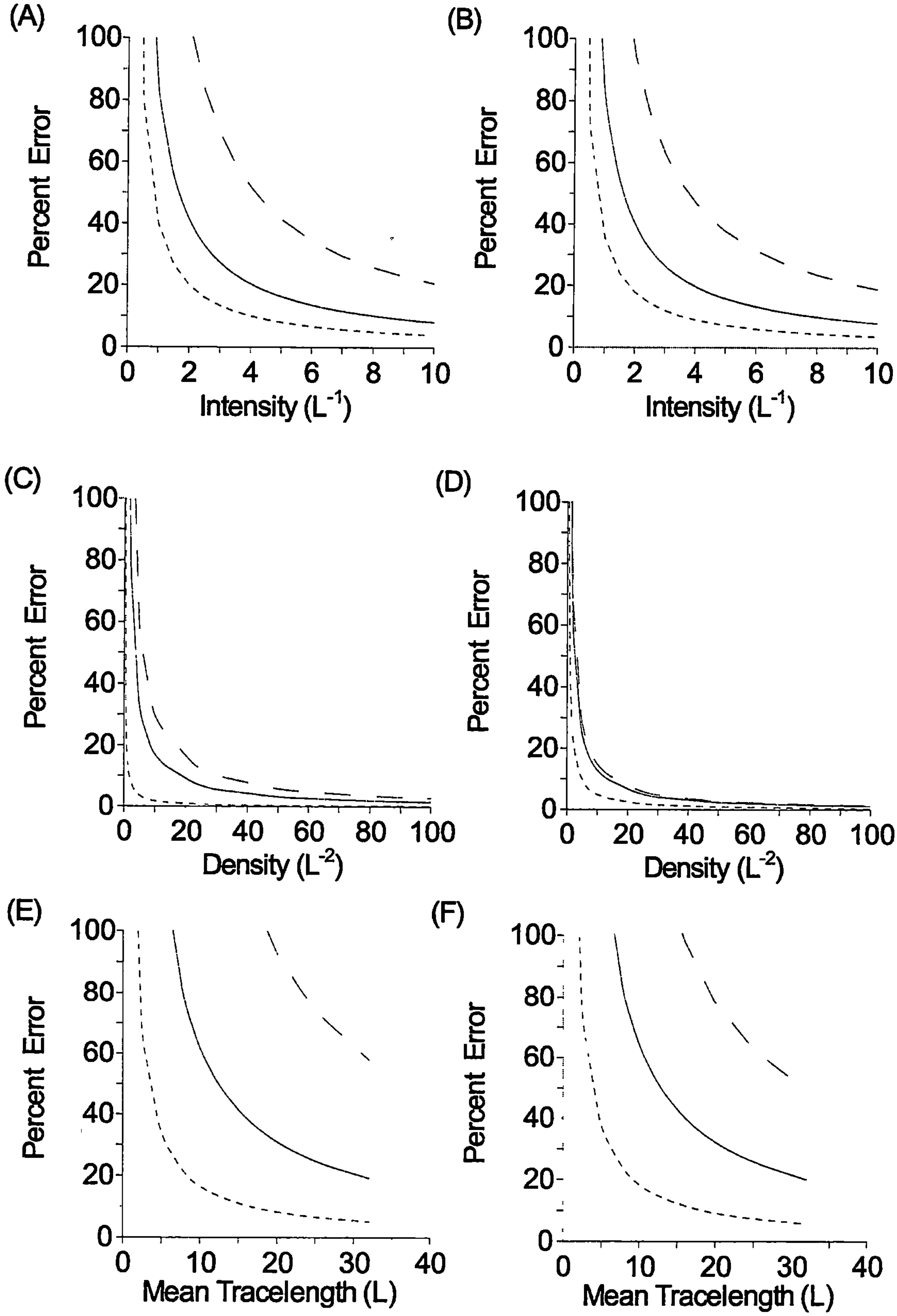
(A)
(B)
(C)
(D)
(E)
(F)
Percent Error
Intensity (L^{-1})
Density (L^{-2})
Mean Tracelength (L)
0
20
40
60
80
100
2
4
6
8
10
30

grid, the effects of clustering are averaged out and the pattern is statistically homogenous. By averaging the effects of clustering, large circles, which are analogous to the large sampling grid, record the least variability and hence yield the smallest delta values (Figures 20C, 21C, 22C).

Figure 24 also illustrates the influence of spatial heterogeneity through clustering, by plotting error bars based on the standard deviation of 100 intensity and density estimates using circles of radius 3 L (open diamonds) and 10 L (solid diamonds). The standard deviation of the estimator increases with smaller circles and/or with lesser intensity or density because the smaller samples less effectively average spatial heterogeneities. Tracelength estimates would illustrate a similar effect.

Minimum Count of m for Reliable Tracelength Estimates

Tracelength estimates are particularly affected by the total count of endpoints (*m*) because this parameter is in the denominator of the estimator (Equation 3). Figure 22A illustrates this effect for a sampling scheme of 6 circles of radius 2 L. For an input mean length greater than 15 L, the error of the estimate increases dramatically. In fact, it is the estimates for larger mean tracelengths that are causing the ΔMTL to be almost equal to 20 (Figure 22C). This increase correlates to a decrease in *m* with increasing L for a fixed intensity, as *m* ranges from 631 to 22 for less than 15 L and from 20 to 6 for greater than 15 L.

Low trace densities or small total sample areas can lead to small values of *m*, and consequently, to poor estimates of mean tracelength (e.g., Figure 22A, Table 5). To

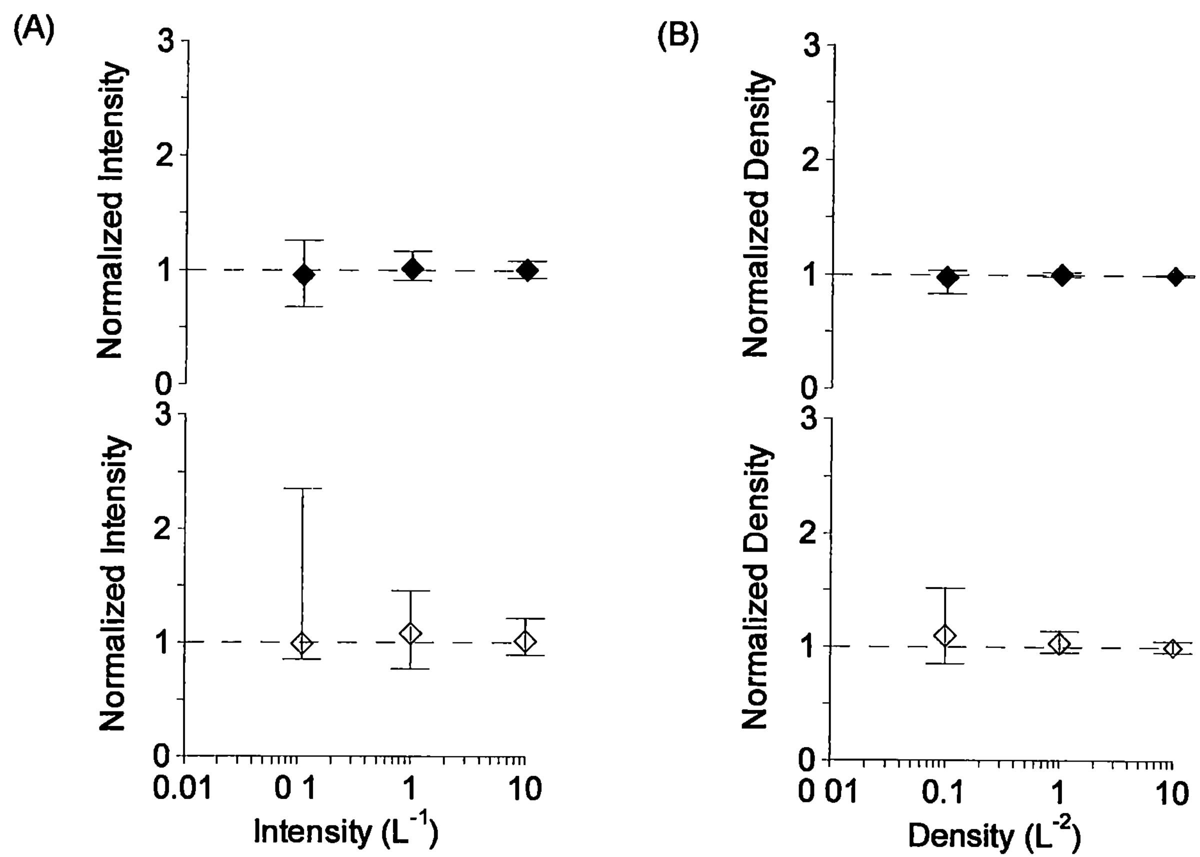

Figure 24 - Normalized standard deviation plots of intensity and density estimates for synthetic patterns. (A) Plots of intensity estimates normalized by the input intensity for circular scanlines of radius 3 L (open diamonds) and 10 L (solid diamonds). Each data point has error bars based on the standard deviation of the normalized intensities for 100 circles of radius 3 L and 10 L. (B) Plots of density estimates normalized by the input density for circular windows of radius 3 L (open diamonds) and 10 L (solid diamonds). Each data point has error bars based on the standard deviation of the normalized densities for 100 circles of radius 3 L and 10 L.

determine a sufficient value of *m* for reliable tracelength estimates, information about the distribution of *m* is needed. Mean *m*, in all cases, is the product of trace density and sample area, multiplied by 2 because each trace has two endpoints. Typical frequency histograms of *m*, obtained from Monte Carlo simulations, are shown in Figures 25A and B. Figure 25A is an approximately normal distribution of *m* with a mean of 16 and a coefficient of variation (COV) of 0.24, whereas Figure 25B is a skewed distribution with a mean of 0.6 and a COV of 1.3. The COV, defined as standard deviation divided by mean, is a normalized measure of the spread of a distribution (e.g., Ang and Tang, 1975). A larger COV results in greater variance in the estimates. For example, mean tracelength estimates for 6 circles ranged from 15 to 25 L when sampling the normal *m* distribution (with a COV of 0.24) and ranged from 8 to 90 L when sampling the skewed *m* distribution with a COV of 1.3 (Figure 25A, B). In both cases, the true mean was 20 L. Thus, an issue becomes constructing a sampling scheme that provides a sufficiently large mean *m* to accurately estimate mean tracelength.

Loss of accuracy in the mean tracelength estimator, when *m* is small, results from the nonlinearity of the estimator (Figure 25C). As shown by this plot, the estimator is highly nonlinear (the rate of change of the slope departs significantly from zero) for *m* less than 6. Thus, to return a value of *m* that yields a reliable estimate of mean tracelength, a sampling scheme is necessary that consistently yields *m* values of 6 or greater. Recognizing that useful sampling schemes produce normal distributions for *m* (Figure 25A), a mean *m* of 20, at a minimum, is needed to insure that 99% of the data (i.e., 3 standard deviations) are greater than 6. The required $\overline{m}$ of 20 is calculated from

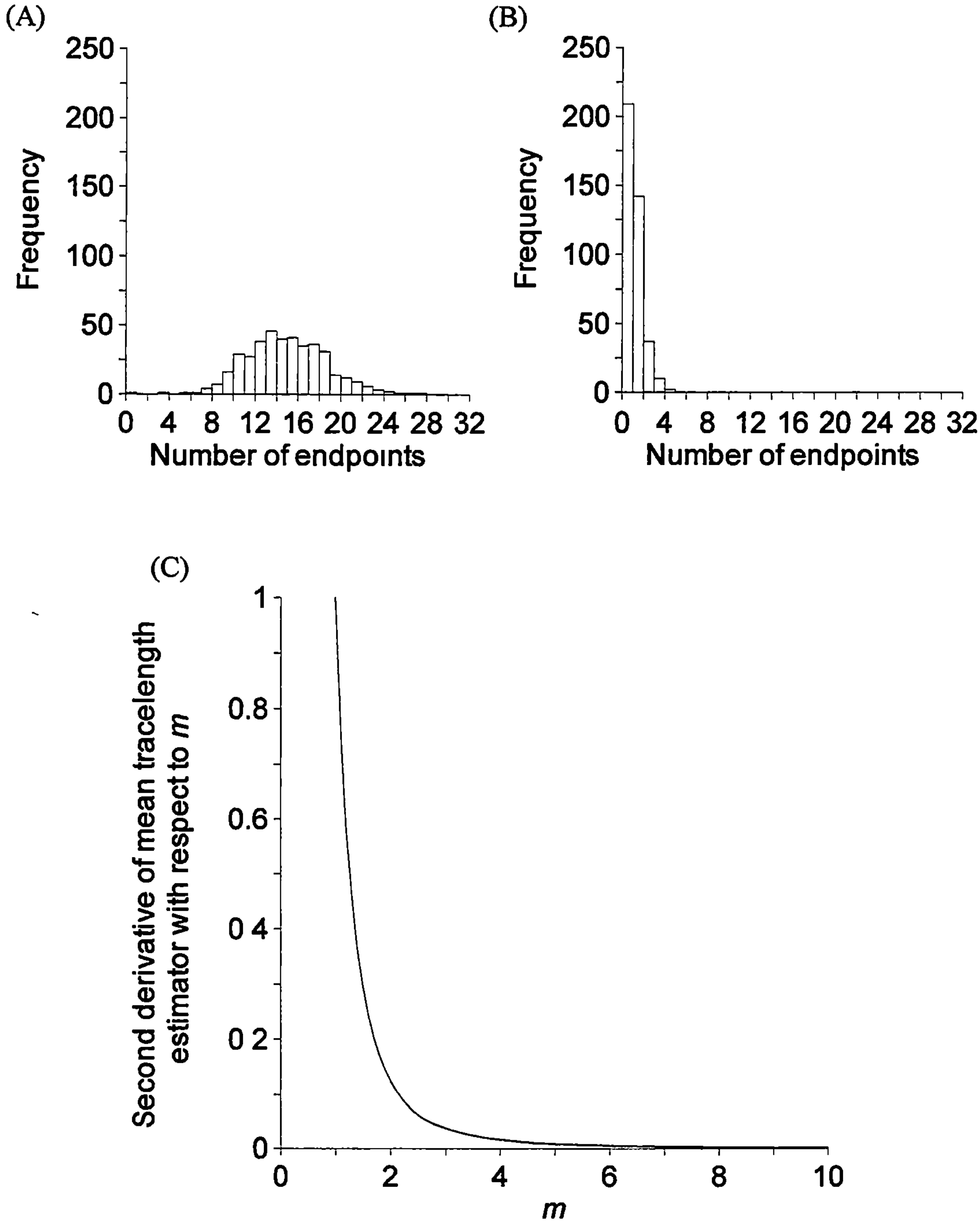

Figure 25 - Determination of the critical value of *m*. (A) Frequency plot of *m* determined from 400 circular windows of radius 1 L sampling a pattern of intensity 2 L^{-1} and density 0.1 L^{-2}. (B) Frequency plot of *m* determined from 400 circular windows of radius 5 L sampling a pattern of intensity 2 L^{-1} and density 0.1 L^{-2}. (C) Plot of second derivative illustrating nonlinearity of mean tracelength estimator.

$$\overline{m} - 3\sigma \geq 6, \quad (6)$$

where σ is the standard deviation. The standard deviation of a Poisson distribution is equal to the $\sqrt{\overline{m}}$. Solving equation 6 for the required $\overline{m}$ produces the value 20, which is similar to the breakdown value of m in Figure 22A. For that case, m values less than 22 caused tracelength estimates to deviate significantly from the perfect prediction line.

A specific sample area is required to produce an $\overline{m}$ of 20 for a given trace density. A plot of density versus total sample area, for an $\overline{m}$ of 20, is shown in Figure 26A. For example, with a trace density of 2 L^{-2}, an area of 5 L^2 is needed, on average, to achieve an $\overline{m}$ of 20. The geometry of the sample area is much less important than the total sample area size. For example, 1 circle of radius 1.26 L and 4 circles of radius 0.63 L both have a sample area of 5 L^2 and yield similar populations of sampled m values (Figure 26B, C). It should be noted that the analysis used to determine the minimum $\overline{m}$ is for fracture traces whose centers follow a Poisson distribution. As a result, $\overline{m} \geq 20$ may not be directly applicable to natural patterns, for which trace centers do not follow a Poisson distribution. Therefore, when characterizing fracture trace geometry, sampling strategies should be designed to yield sufficient m for reliable estimates of mean tracelength.

Summary

Plots of prediction intervals (PI) for estimated values of fracture characteristics provide a means of bounding the range of likely predicted values from a fracture pattern at the 95% confidence level. The PI plots for intensity, density and mean tracelength show that the prediction interval is reduced more effectively by increasing circle radius

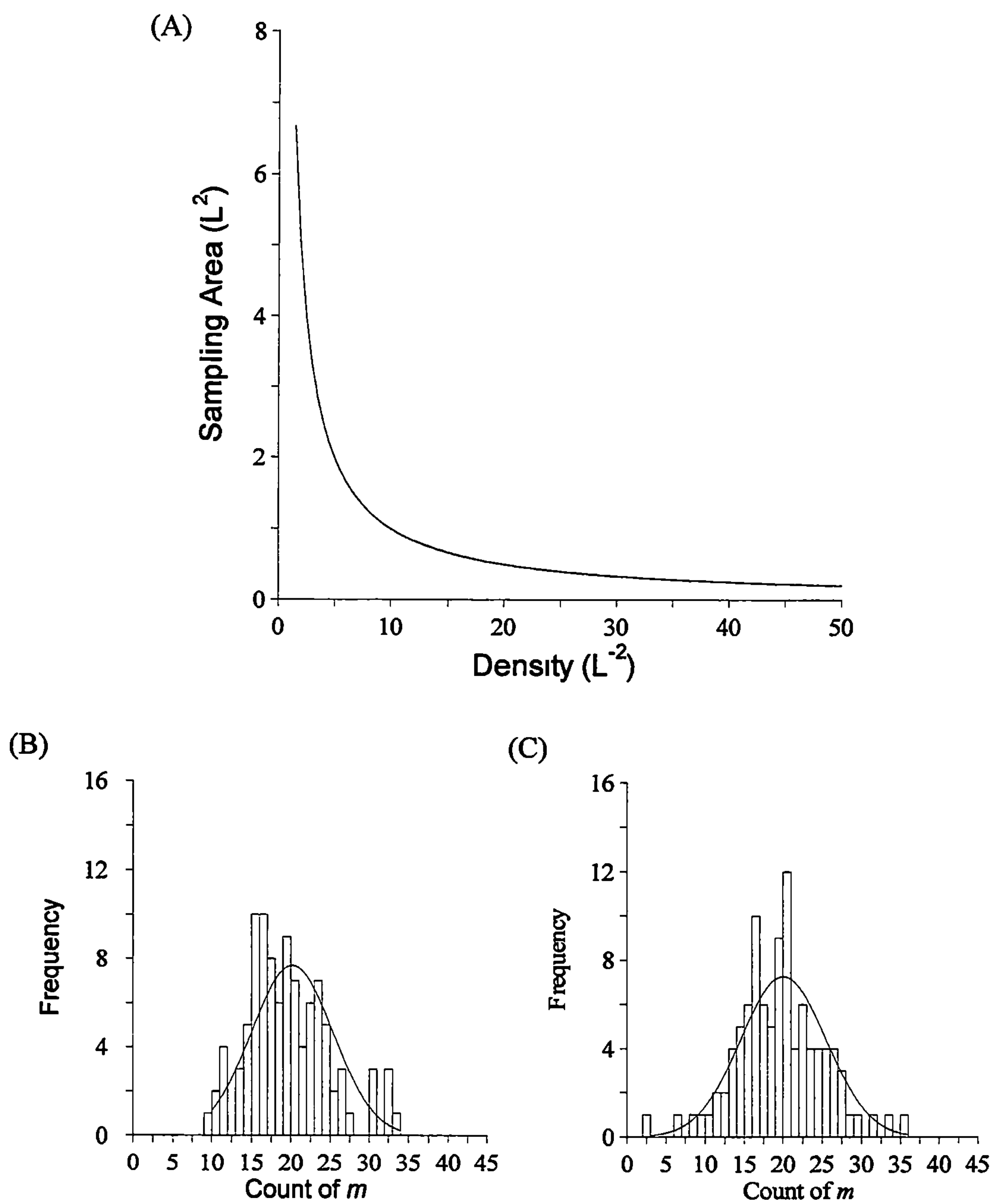

Figure 26 - Determination of minimum sampling area for tracelength estimates. (A) Plot of sampling area versus fracture density. Solid line represents values within 3 standard deviations ($m = 20$) (B) Frequency plot of 100 counts of total m determined from using 1 circular window of radius 1.26 L sampling a fracture pattern of intensity 10.0 L^{-1} and density 2.0 L^{-2}. (C) Frequency plot of 100 counts of total m determined using 4 circular windows of radius 0.63 L sampling a fracture pattern of intensity 10.0 L^{-1} and density 2.0 L^{-2}.

rather than increasing the number of circles. Larger circle radii perform better than greater numbers of small circles because the larger circles average out the effects of spatial heterogeneity more effectively. The narrowness of the PI and hence the quality of the estimate for tracelength is also improved by designing sampling strategies that favor large values of *m*. For trace centers that follow a Poisson point process, sampling schemes should be designed to produce an $\overline{m} \geq 20$. This value, however, should not be applied literally to natural patterns, whose fracture centers may not follow a Poisson distribution. The general principle is that the estimators produce better results with sampling strategies that achieve large counts of trace endpoints.

Natural Fracture Patterns

Having developed the 95% PI from synthetic patterns, the applicability of these predictions intervals to natural patterns was tested. Forty sets of a sampling scheme for estimating intensity was applied to the cross joints at Llantwit Major. The estimates were compared to the intensity values determined by areal sampling of the cross joints across the entire pavement, which was taken as a baseline estimate (Figures 14A, 15). All estimates plot well inside the 95% PI derived from the synthetic patterns (Figure 27). Rather than being simply good fortune, these results are interpreted to indicate that the degree of clustering is less in the natural case examined than for the synthetic cases used to construct the 95% PI. A test of clustering for the cross joints at Llantwit Major, using counts of fracture centers for a grid containing 36 cells of dimensions 1 m by 1 m, indicates that the fractures are only slightly clustered because the variance (6.0) is slightly

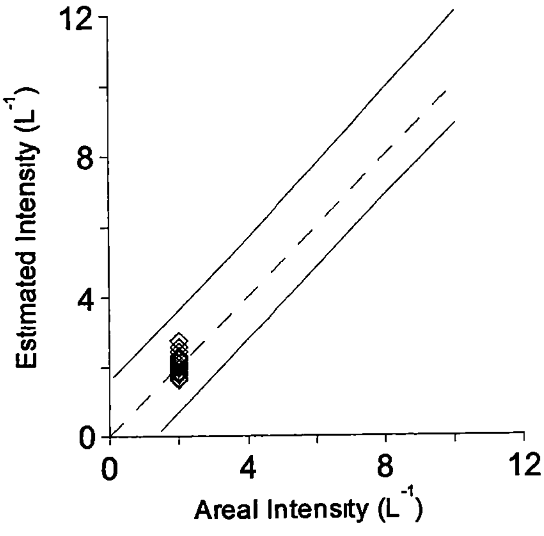

Figure 27 - Superposition of synthetic 95% PI for intensity (solid lines) and data points for intensity estimates for the Llantwit Major cross joints using a sampling scheme of 6 circles of radius 2 m.

larger than the mean (5.4). Fracture centers were used instead of endpoints because the endpoints of the cross joints are anisotropically clustered, causing clustering estimates to be in error. Variations due to clustering were further reduced, in comparison with the 1 m grid, by using a 2 m radius circular scanline, with the result that all 40 intensity estimates plotted well inside the 95% PI derived from synthetic patterns. Again, increasing circle size reduces spatially heterogeneities related to clustering and thus improves the accuracy of estimates of average fracture intensity for natural patterns.

To narrow the range of predicted intensities for natural patterns, and hence improve the accuracy of the estimator, 9 natural joint sets or patterns were examined (Table 1, Figures 4-10). For each natural population of fracture traces, a homogeneous subdomain, in terms of intensity, was visually identified (Figures 4-10). The areal intensities for the 9 sampled trace patterns are shown in Table 6. These trace populations range in intensity from 0.50 to 3.6 m^{-1}. The range of intensities sampled comes from a variety of lithologies and structural settings, and thus are interpreted as being representative of natural trace patterns (e.g., Hancock, 1985; Pollard and Aydin, 1988; Barton, 1995).

Similar to the analysis for synthetic fracture traces, the 95% PI plots for 20 sampling strategies were summarized as maximum ΔI plots (Figure 28C) because ΔI was approximately constant over the range analyzed (e.g., Figure 28A, B). Again, like the synthetics, ΔI generally decreases with increasing circle radius and increasing number of circles, with the greatest reduction occurring with increasing radius (Figure 28C). Again, the greater effect of increasing radius illustrates the effect of increasing the size of the

Table 6. Intensities and "Blockiness" for Natural Fracture Patterns

Natural Fracture Patterns*	Baseline Intensity (m^{-1})**	"Blockiness"
Llantwit Major, cross joints	2.0	Ladder pattern blocks (Figure 4)
Llantwit Major, master joints	3 4	
Amroth, 200° set	1.8	Rectangular blocks with 290° set (Figure 5)
Amroth, 316° set*	0.55	
Rocky Creek, all fractures*	3.3	No blockiness (Figure 7)
Telpyn Point, 200° set	3.6	Poor blockiness (Figure 8)
Telpyn Point, 290° set	0.50	
Ward Lake, 015° set*	1.0	No blockiness (Figure 9)
P100, YM[+], all fractures*	2.8	No blockiness (Figure 10)

*refers to pavements where only the lightly stippled region was sampled for the analysis
**Baseline intensity was measured for the entire target area using areal sampling
[+]Yucca Mountain, Nevada

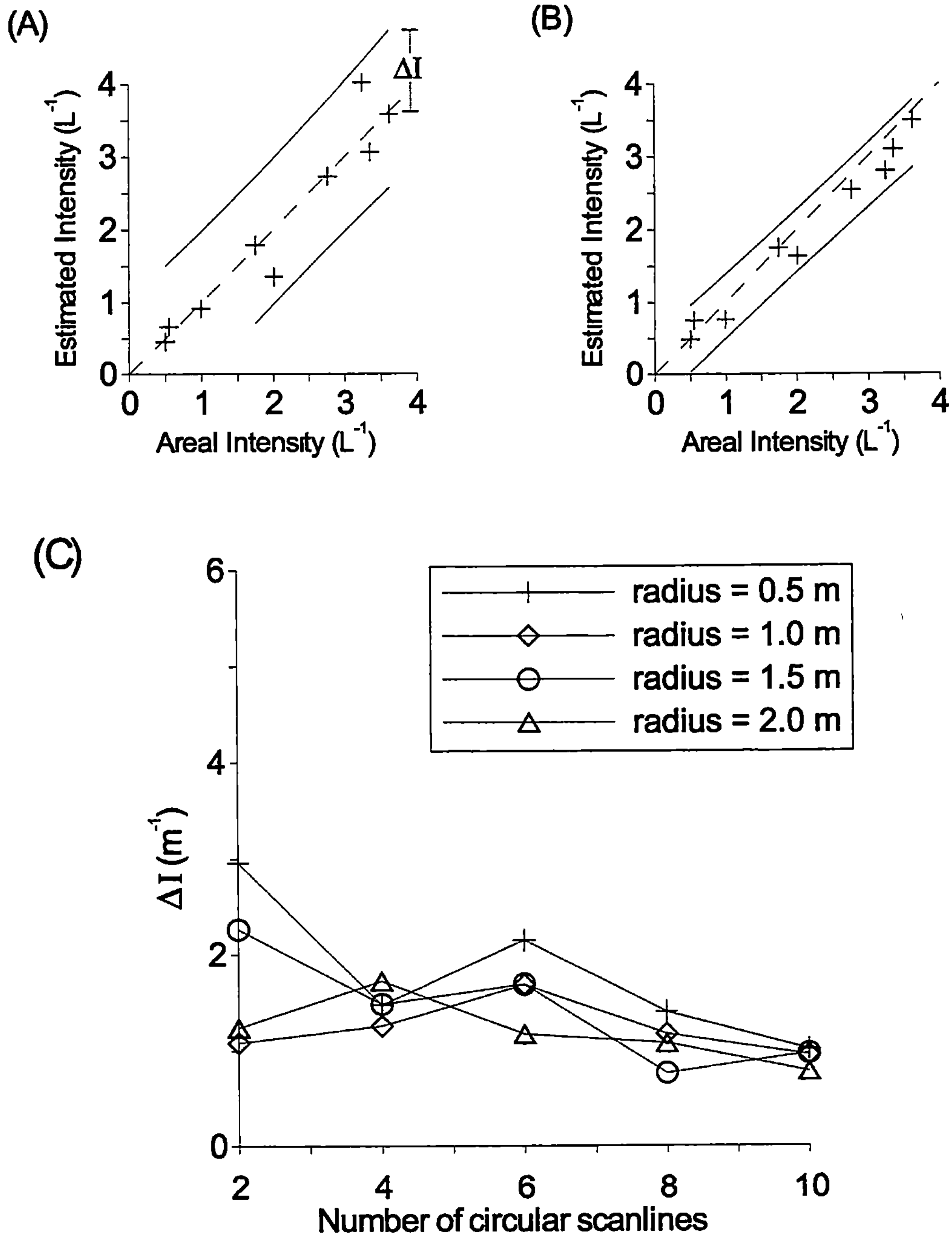

Figure 28 - Prediction intervals for intensity estimates from natural patterns. (A) 95% PI plot for average intensity estimates (plus signs) from 6 circles of radius 2.0 m. (B) 95% PI plot for average intensity estimates (plus signs) from 10 circles of radius 2.0 m. (C) Plot of ΔI for 20 sampling strategies for natural fracture traces. Dashed lines in (A) and (B) represents a perfect prediction; black lines in (A) and (B) represents upper and lower 95% PI.

sample tool with respect to the scale of spatial heterogeneities due to clustering.

A similar analysis to determine 95% PI for the density and mean tracelength estimators, based on natural pavements, could not be performed because the true values of density and mean tracelength are unknown in natural patterns due to censoring and length bias (Figures 14B, C, 16, 17).

5. DISCUSSION

Comparative Efficiency of the New Circle-based Estimators and Areal Sampling

One of the claims made in this paper is that estimates from the new circular sampling tools can be obtained much more quickly than estimates from construction of fracture trace maps. In support of this claim, this section provides data on the time it took to construct fracture trace maps at three of the sites discussed in this thesis: the rock pavements at Llantwit Major, Amroth and Telpyn Point (Figures 4, 5, 8). A team of three, of whom two were experienced fracture mappers, manually constructed trace maps for these pavements. The Llantwit Major pavement was mapped under ideal weather conditions in a total of 26 person-hours with a minimum mapped fracture size (truncation limit) of 0.2 m. The Amroth and Telpyn Point pavements were mapped in 36 person-hours (truncation limit = 0.4 m) and 52 person-hours (truncation limit = 0.4 m), respectively, in a light rain. The Llantwit Major pavement is horizontal, the Amroth and Telpyn pavements have gentle dips of less than 15°S.

Collecting values of n and m for 10 circles of radius 2 m, on the other hand, would typically require less than 2 hours per pavement. While it might be possible to reduce the time required for constructing a trace map by using GPS equipment with real-time correction capability, data processing would still be required. Furthermore, such equipment is substantially more expensive than a string, piece of chalk, a tape measure, and a calculator with a random-number generator.

It should be remembered that while the use of the circle-based estimators is not a substitute for a fracture trace map when the exact pattern geometry is needed, these new tools are still needed for reliable estimates of density and mean tracelength. As discussed earlier, the estimates may be collected by making a digital version of the map and importing it into JAWS, which is freely available from the authors.

Achieving Independence between Sampling Tools and the Exposed Fracture Pattern

A basic principle for any sampling technique is that samples should be random and independent of the geometry of the target population of fracture traces. Circular or straight scanlines, for example, should be positioned without regard for fracture trace locations. While this principle is relatively easy to achieve for scanlines or windows, the requirement may not hold for exposed areas with boundaries either coincident with, or controlled by, natural fractures. For example, the southern border of the Llantwit Major pavement (Figure 4) is partly formed by cross joints. Similar relationships occur for the Amroth and Telpyn Point pavements (Figures 5 and 8). Such a coincidences of pavement boundaries and fractures skews whole-sample areal measures of fracture characteristics. For these pavements, fractures that coincided with the boundary were excluded from the whole-sample estimates. It should be noted that the sampling techniques proposed in this thesis, namely circular scanlines and windows, are not affected by any lack of independence between exposed pavement area and the fracture network.

Effects of Block Size on Estimates

Block size refers to the dimensions of an unfractured area in a fracture pavement containing two or more fracture sets (LaPointe, 1988). Block size controls the degree of clustering because both clustering and block size measure variation in the degree of separation of fractures in a natural fracture pattern. The effect of block size on intensity estimates was investigated for Llantwit Major and for the stippled portion of Amroth. The mean block size at Llantwit Major is approximately 0.7 to 1 m by 0.3 to 0.5 m, whereas at Amroth the mean block size between the 200° and 290° sets is approximately 2.5 by 1 m. Figure 29A shows that using circle sizes smaller than mean block size (radius of 0.10 m for Llantwit Major, 0.25 m for Amroth) produces large standard deviations in the intensity estimates, whereas Figure 29B shows that using circles larger than mean block size (radius of 0.75m for Llantwit Major, 1.5 m for Amroth) produces significantly smaller standard deviations. Therefore, a recommendation of this study for natural patterns with a "blocky" character (Table 6) is to use a circle size that noticeably exceeds block dimensions so as to reduce error in intensity estimates due to clustering. Such a sampling scheme would also increase the accuracy of estimates for density and mean tracelength.

Application to 3D Seismic Volumes

Circular scanlines and windows, in this thesis, have been applied to joint patterns in 2D. In reality, these estimators can be used to sample any linear feature. For example, using 3D seismic volumes (e.g., Apotria and Hudec, 1997), the estimators could be used to determine the intensity, density and mean length of faults that intersect a surface in the cube. By using the estimators on mutually orthogonal surfaces within a 3D seismic cube, one could approximate these fracture characteristics in three dimensions. Also, one could

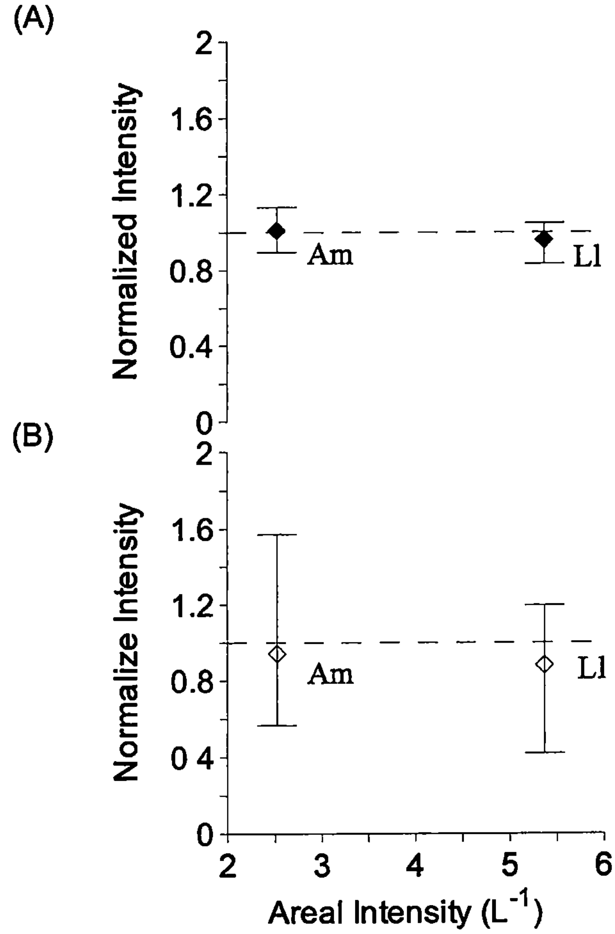

Figure 29 - Plots of intensity estimates normalized by the average areal intensity for the 200°and 290° sets in the stippled portion of Amroth (Am in figure; I = 2.5 m^{-1}) and the master and cross joints at Llantwit Major (Ll in figure; I = 5.4 m^{-1}). Data points with error bars based on the standard deviation of the normalized intensity for 100 circles. (A) Radii larger than block size. (B) Radii smaller than block size.

determine how these parameters change as a function of depth or along strike by sampling various surfaces within the cube.

6. CONCLUSIONS

(1) New distribution-independent estimators of intensity, density and mean tracelength, using circular scanlines and windows, successfully handle orientation bias, censoring and length bias, which plague the straight scanline and area methods.

(2) When applied to synthetic and natural patterns, the estimates of intensity, density and mean tracelength accurately represent the population values. For the cases of density and mean tracelength, the estimators perform more accurately than apparent density and apparent mean tracelength. The accuracy of the estimates improves (variance decreases) as the sample size increases.

(3) Plots of prediction intervals (PI) based on estimates of intensity, density and mean tracelength provide a means of bounding the range of likely predicted values from a fracture pattern at the 95% confidence level. The PI plots show that greater quality is achieved by increasing circle radius rather than by increasing circle number, because the increasing radius averages out the effects of clustering.

(4) For mean tracelength estimates, counts of trace endpoints lower than 6 cause the estimator to breakdown because the estimator is nonlinear. To insure that a minimum value of 6 is exceeded with 99% probability, a sampling scheme should be designed so as to produce an $\overline{m} \geq 20$. A specific $\overline{m}$, for a given density, is achieved by specifying the total sample area. The recommended $\overline{m}$ of 20 should not be applied literally to natural patterns, whose fracture centers may not follow a Poisson distribution, but this analysis does emphasize the need to design sampling strategies to achieve larger counts of endpoints.

(5) These estimators are extremely time efficient because they only require knowledge of n and m, as opposed to constructing a full trace map.

REFERENCES CITED

Amadei, B. and W.Z. Savage, 1993, Effects of joints on rock mass strength & deformability, in J. A. Hudson ed., Comprehensive Rock Engineering: New York, Pergamon, v. 1, p. 331-365.

Anna, L.O. and P. Wallman, 1997, Characterizing the fracture network at Yucca Mountain, Nevada. Part 2: Numerical simulation of flow in a three-dimensional discrete fracture pattern, in T.E. Hoak, A.L. Klanwitter and P.K. Blomquist eds., Fracture Reserviors: Characterizing and Modeling: Denver, Colorado, The Rocky Mountain Association of Geologist, p. 199-207.

Ang, A.H-S. and W.H. Tang, 1975, Probability concepts in engineering planning and design, vol. 1: New York, John Wiley.

Apotria, T. and M. Hudec, 1997, Controls on displacement transfer and fault linkage in salt-detached fault systems, Gulf of Mexico, in Geological Society of America Abstracts with Programs, v. 29, p. 199.

Baecher, G.B., 1980, Progressively censored sampling of rock joint traces: Mathematical Geology, v. 12, p. 33-40.

Baecher, G.B. and N.A. Lanney, 1978, Trace length biases in joint surveys, in Proceedings of the 19th U.S. Symposium on Rock Mechanics: Lake Tahoe, Nevada, v. 1, p. 56-65.

Barton, C.C., 1995, Fractal analysis of scaling and spatial clustering of fractures, in C.C. Barton and P.R. LaPointe eds., Fractals in the Earth Sciences: New York, Plenum Press, p. 141-178.

Barton, C.C., E. Larsen, W.R. Page and T.M. Howard, 1993, Characterizing fractured rock for fluid-flow, geomechanical, and paleostress modeling: Methods and preliminary results from Yucca Mountain, Nevada: United States Geological Society Open-File Report 93-269, 62 p.

Bear, J., C.-F. Tsang and G. de Marsily, 1993, Flow and Contaminant Transportation in Fractured Rock: San Diego, California, Academic Press.

Becker, A. and M.R. Gross, 1996, Mechanism for joint saturation in mechanically layered rocks: an example from southern Israel: Tectonophysics, v. 257, p. 223-237.

Bowerman, B.L. and R.T. O'Connell, 1990, Linear Statistical Models: an applied approach, 2nd ed.: Belmont, California, Duxbury Press.

Cruden, D.M., 1977, Describing the size of discontinuities: International Journal of Rock Mechanics and Mining Sciences and Geomechanical Abstracts, v. 14, p. 133-137.

Davis, G.H. and S.J. Reynolds, 1996, Structural Geology of Rocks and Regions: New York, John Wiley and Sons, Inc., p. 724-726.

Davis, J.C. 1986, Statistics and Data Analysis in Geology, 2nd ed.: New York, John Wiley and Sons.

Dershowitz, W.S. and H.H. Einstein, 1988, Characterizing rock joint geometry with joint system models: Rock Mechanics and Rock Engineering, v. 21, p. 21-51.

Dershowitz, W.S. and H.H. Herda, 1992, Interpretation of fracture spacing and intensity: in J.R. Tillerson and W.R. Wawersik *eds.,* Proceeding of the 33rd U.S. Symposium on Rock Mechanics: Rotterdam, Balkema, p. 757-766.

Dershowitz, W.S. and P.R. LaPointe, 1994, Discrete fracture approaches for oil and gas applications, in R.A. Nelson and S. Laubach eds., Rock Mechanics: Rotterdam, Balkema, p. 19-30.

Dunne, W.M. and C.P. North, 1990, Orthogonal fracture systems at the limits of thrusting: an example from southwestern Wales: Journal of Structural Geology, v. 12, p. 207-215.

Ehlen, J., 1998, Matching simulated fracture data with field measurements using joint intensity: International Journal of Rock Mechanics and Mining Sciences and Geomechanical Abstracts, v. 35, p. 504, Paper No. 10.

Einstein, H.H. and G.B. Baecher, 1983, Probablistic and statistical methods in engineering geology, specific methods and examples, part 1: exploration: Rock Mechanics and Rock Engineering, v. 16, p. 39-72.

Fossum, A.F., 1985, Effective elastic properties for a randomly jointed rock mass: International Journal of Rock Mechanics and Mining Sciences and Geomechanical Abstracts, v. 22, p. 467-470.

Ghosh, A. and J.J.K. Daemen, 1993, Fractal characteristics of rock discontinuities: Engineering Geology, v. 34, p. 1-9.

Gilmour, H.M.P., D. Billaux and J.C.S. Long, 1986, Models for calculating fluid flow in randomly generated three-dimensional networks of disk-shaped fractures: theory and design of FMG3D, DISCEL and DIMES. Lawrence Berkeley Laboratory, Earth Sciences Division, LBL-19515.

Goodman, R.E. and G. Shi, 1985, Block theory and its application to rock engineering: New Jersey, Prentice Hall Inc.

Hancock, P.L, 1985, Brittle microtectonics; principles and practice: Journal of Structural Geology, v. 7, p. 437-457.

Hammersley, J.M. and D.C. Handscomb, 1965, Monte Carlo methods: London, Chapman Hall.

Hoek, F. and J.W. Bray, 1977, Rock Slope Engineering, 2nd ed.: London, The Institute of Mining and Metallurgy.

Hocking, R.R., 1996, Methods and Applications of Linear Models: Regression and the Analysis of Variance: New York, John Wiley & Sons, Inc.

Hu, K.X. and Y. Huang, 1993, Estimation of elastic properties of fractured rock masses: International Journal of Rock Mechanics and Mining Sciences and Geomechanical Abstracts, v. 30, p. 381-394.

Jaeger, J.C. and N.G.W. Cook, 1969, Fundamentals of Rock Mechanics: London, Methuen.

Jian, X., R. Olea and Y. Yu, 1996, Semivariogram modeling by weighted least square: Computers and Geosciences, v. 22, p. 387-397.

Kulatilake, P.H.S.W. and T.H. Wu, 1984a, Estimation of mean trace length of discontinuities: Rock Mechanics and Rock Engineering, v. 17, p. 215-232.

Kulatilake, P.H.S.W. and T.H. Wu, 1984b, The density of discontinuity traces in sampling windows (Technical Note): International Journal of Rock Mechanics and Mining Sciences and Geomechanical Abstracts, v. 21, p. 345-347.

Kulatilake, P.H.S.W., S. Wang and O. Stephansson, 1993a, Effect of finite size joints on deformability of jointed rock at the three-dimensional level: International Journal of Rock Mechanics and Mining Sciences and Geomechanical Abstracts, v. 30, p. 479-501.

Kulatilake, P.H.S.W, D.N. Wathugala and O. Stephansson, 1993b, Joint network modeling with a validation exercise in Stripa Mine, Sweden: International Journal of Rock Mechanics and Mining Sciences and Geomechanical Abstracts, v. 30, p. 503-526.

Kulatilake, P.H.S.W., J. Chen, J. Teng, X. Shufang and G. Pan, 1996, Discontinuity geometry characterization in a tunnel close to the Three Gorges dam site in China: International Journal of Rock Mechanics and Mining Sciences and Geomechanical Abstracts, v. 33, p. 255-277.

Kulatilake, P.H.S.W., R. Fiedler and B.B. Panda, 1997, Box fractal dimension as a measure of statistical homogeneity of jointed rock masses: Engineering Geology, v. 48, p. 217-229.

LaPointe, P.R., 1988, A method to characterize fracture density and connectivity through fractal geometry: International Journal of Rock Mechanics and Mining Sciences and Geomechanical Abstracts, v. 24, p. 421-429.

LaPointe, P.R., 1993, Pattern analysis and simulation of joints for rock engineering, in J.A. Hudson ed., Comprehensive Rock Engineering, Volume 3 - Rock testing and site characterization: New York, Pergamon Press, p. 215-239.

LaPointe, P.R. and J.A. Hudson, 1985, Characterization and interpretation of rock mass joint patterns: Geological Society of America Special Paper, v. 199, 37 p.

Lacazette, A., 1991, A new sterographic technique for the reduction of scanline survey data of geologic fractures: Computers and Geosciences, v. 17, p. 445-463.

Long, J.C.S and P.A. Witherspoon, 1985, The relationship of the degree of interconnection of permeability in fracture networks: Journal of Geophysical Research, v. 90, p. 3087-3098.

McKay, L.D., J.A. Cherry and R.W. Gillham, 1993, Field experiments in a fractured clay till, 1, hydraulic conductivity and fracture aperature: Water Resources Research, v. 29, p. 1149-1162.

Maritz, J.S., 1981, Distribution-free statistical methods: London, Chapman Hall.

Mauldon, M., 1994, Intersection probabilities of impersistent joints: International Journal of Rock Mechanics and Mining Sciences and Geomechanical Abstracts, v. 31, p. 107-115.

Mauldon, M., 1998, Estimating mean fracture trace length and density from observations in convex windows: Rock Mechanics and Rock Engineering, v. 31, p. 201-216.

Mauldon, M. and J.G. Mauldon, 1997, Fracture sampling on a cylinder: from scanlines to boreholes and tunnels: Rock Mechanics and Rock Engineering, v. 30, p. 129-144.

Mauldon M., M.B. Rohrbaugh Jr., W.M. Dunne and W. Lawdermilk, 1999a, Fracture intensity estimates using circular scanlines, in B. Amadei, R.L. Kranz, G.A. Scott and P.H. Smeallie eds., Proceedings of the 37th US Rock Mechanics Symposium: Rock Mechanics for Industry: Rotterdam, Balkema, p. 777-784.

Mauldon, M., M.B. Rohrbaugh Jr., W.M. Dunne and W. Lawdermilk, 1999b, Estimators for mean fracture trace length and density using circular windows, in B. Amadei, R.L. Kranz, G.A. Scott and P.H. Smeallie eds., Proceedings of the 37th U.S. Rock Mechanics Symposium: Rock Mechanics for Industry: Rotterdam, Balkema, p. 785-792.

Mauldon, M. M.B. Rohrbaugh Jr., W.M. Dunne, in review, Circular scanlines and circular windows: New tools for characterizing the geometry of fracture traces: Journal of Structural Geology.

Mecke, J., 1981, Formulas for stationary planar fibre processes III - intersections with fibre systems: Mathematische Operationsforschung und Statistik. Series Statistik, v. 12, p. 201-210.

Narr, W., 1996, Estimating average fracture spacing in subsurface rock: The American Association of Petroleum Geologists, v. 80, p. 1565-1586.

Nelson, R.A., 1985, Geologic Analysis of Naturally Fractured Reservoirs: Houston, Texas, Gulf Publishing Co.

Nemcock, M., R. Bayer and M. Miliorizos, 1995, Structural analysis of the inverted Bristol Channel Basin: implications for the geometry and timing of fracture porosity, in J.G. Buchanan and P.G. Buchanan eds., Basin Inversion: London, Geological Society of London, Special Publication, v. 88, p. 355-392.

Pahl, P.J., 1981, Estimating the mean length of discontinuity traces: International Journal of Rock Mechanics and Mining Sciences and Geomechanical Abstracts, v. 18, p. 221-228.

Panek, L.A., 1985, Estimating fracture trace length from censored measurements of multiple scanlines, in O. Stephansson ed., Proceedings of the International Symposium on Fundamentals of Rock Joints: Centek, Bjorkliden, p. 13-23.

Parker, P. and R. Cowan, 1976, Some properties of line segment processes: Journal of Applied Probability, v. 13, p. 96-107

Pickering, G., J.M. Bull and D.J. Sanderson, 1995, Sampling power-law distributions: Tectonophysics, v. 248, p. 1-20.

Pollard, D.D and A. Aydin, 1988, Progress in understanding jointing over the past century: Geological Society of America Bulletin, v. 100, p. 1181-1204.

Priest, S.D., 1993, Discontinuity Analysis for Rock Engineering: New York, Chapman and Hall, p. 50-54.

Priest, S.D. and J.A. Hudson, 1981, Estimation of discontinuity spacing and trace length using scanline surveys: International Journal of Rock Mechanics and Mining Sciences and Geomechanics Abstracts, v. 18, p. 183-197.

Rawnsley, K.D., D.C.P. Peacock, T. Rives and J.-P. Petit, 1998, Joints in the Mesozoic sediments around the Bristol Channel Basin: Journal of Structural Geology, v. 20, p. 1641-1661.

Reiss, L.H., 1982, The reservoir engineering aspects of fractured formations: Houston, Texas, Gulf Publishing, 186 p.

Rouleau, A. and J.E. Gale, 1985, Statistical characterization of the fracture system in the Stripa Granite, Sweden: International Journal of Rock Mechanics and Mining Sciences and Geomechanics Abstracts, v. 22, p. 353-367.

Santal6, L.A., 1976, Integral Geometry and geometric probability: Reading, MA, Addison-Wesley.

Segall, P. and D.D. Pollard, 1983, Joint formation in granitic rock of the Sierra Nevada: Geological Society of America Bulletin, v. 94, p. 563-575.

Sen, Z. and A. Kazi, 1984, Discontinuity spacing and RQD estimates from finite length scanlines: International Journal of Rock Mechanics and Mining Sciences and Geomechanics Abstracts, v. 21, p. 203-212.

Stoyan, D., W.S. Kendall and J. Mecke, 1995, Stochastic geometry and its applications, 2nd edition: New York, John Wiley and Sons, p. 286-296.

Terzaghi, R.D., 1965, Sources of error in joint surveys: Geotechnique, v. 15, p. 287-304.

Titley, S.R., R.C. Thompson, F.M. Haynes, S.L Manske, L.C. Robison and J.L. White, 1986, Evolution of fractures and alteration in the Sierrita-Esperanza Hydrothermal System, Pima County, Arizona: Economic Geology, v. 81, p. 343-370.

Villaescusa, E. and E.T. Brown, 1992, Maximum Likelihood estimation of joint size from trace length measurements: Rock Mechanics and Rock Engineering, v. 25, p. 67-87.

Wheeler, R.L. and J.M. Dixon, 1980, Intensity of systematic joints: methods and application: Geology, v. 8, p. 230-233.

Wiltschko, D.V., K.P. Corbett, M. Friedman and J.H. Hung, 1991, Predicting fracture connectivity and intensity within the Austin Chalk from outcrop fracture maps and scan line data: Transactions of the Gulf Coast Association of Geological Societies, v. 41, p. 702-718.

Wu, H. and D.D. Pollard, 1995, An experimental study of the relationship between joint spacing and layer thickness: Journal of Structural Geology, v. 17, 887-905.

Yow, J.L., 1987, Blind zones in the acquisition of discontinuity orientation data: International Journal of Rock Mechanics and Mining Sciences and Geomechanical Abstracts, v. 24, p. 317-318.

Zhang, L. and H.H. Einstein, 1998, Estimating the mean trace length of rock discontinuities: Rock Mechanics and Rock Engineering, v. 31, p. 217-234.

Zhang, X. and G. Liao, 1990, Estimation of confidence bounds for mean trace length of discontinuities using scanline surveys (Technical Note): International Journal of Rock Mechanics and Mining Sciences and Geomechanical Abstracts, v. 27, p. 207-212.

APPENDICES

APPENDIX A

JAWS VERSION 1.0 – USER'S MANUAL

1.0 INTRODUCTION

JAWS (Joint Analysis using Windows and Scanlines) is designed to rapidly analyze synthetic and natural fracture pavements using straight scanlines, circular scanlines, and circular windows.

Using this program, estimates of fracture intensity (using straight scanlines, area method and circular scanlines), fracture density (using circular windows), and the mean tracelength (using circular windows) of the fracture population can be determined.

2.0 STARTUP

Before using this program, a **subdirectory** called "C:\Frac" must be created. All data analysis files (FracSet1.txt, FracSet2.txt, FracSet3.txt, and FracSet4.txt) are written to this subdirectory as comma delimited text files. Each data file only contains analysis for a particular fracture set (e.g. FracSet1.txt contains analysis of fracture set 1).

Note: Data is always written to all the files even if that fracture set doesn't exist.
Note: To view the program on your computer monitor, the screen resolution of your computer must be set at 1024 × 768 pixels or higher.

3.0 DATA ENTRY

On the startup screen (Figure A1), under **Data Sources,** the user is given the option to open a ***Real*** fracture pattern (either an Adobe Illustrator file '*.ai' or a text file '*.txt'), generate a ***Synthetic*** fracture pattern, or ***Manual*** entry of the fracture data.

3.1 *Real Data*:

3.1.1 Adobe Illustrator

The user must open a digitized fracture pattern that is in Adobe Illustrator '*.ai' format.

- The file must only contain line art (i.e. **no text and fill colors**).
- The file must contain at least 2 layers, but may contain as many as 5 layers.
- The layer titles must not contain any spaces.
- The bottom layer must be a polygon that was digitized as a series of straight-line segments (no bezier curves) representing the edge of the fracture pattern and/or any covered areas within the fracture pattern.

- The other layers must be fracture traces that were digitized as a series of straight-line segments.

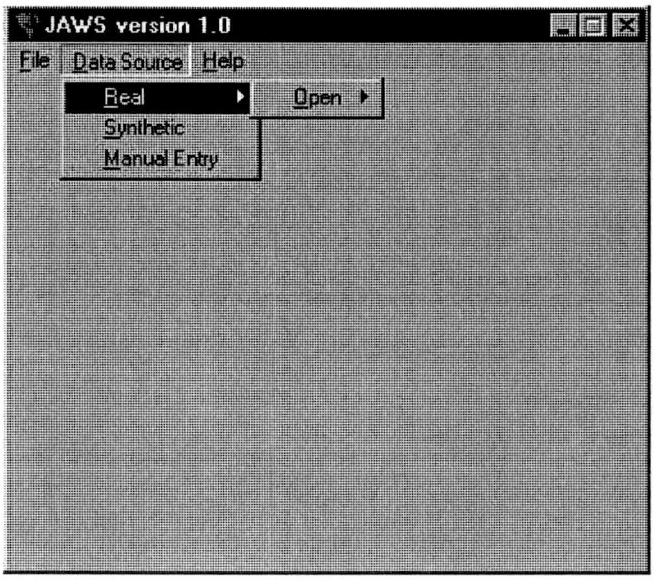

Figure A1. Startup screen that allows the user to select the type of data to be entered

- Once the polygon and the fracture sets are in their appropriate layer, a **cleanup** must be performed. The **cleanup** option is under the **Option→Path→Cleanup** menu in Adobe Illustrator. Check all three boxes (Stray Points, Unpainted Objects, and Empty Text Paths) and press OK. This will get rid of any "invisible" points that will cause JAWS to not load the file properly.
- Before loading the file into JAWS, the scale factor of the fracture pavement must be known. This is determined by calculating how many *points* (you can set the measuring units in Adobe Illustrator to *points* using the **File→Document Setup** menu) are equal to ten units. For example, if 20 *points* are equal to one meter in the fracture pattern, then the scale factor you will need for 10 units (Figure A2) is 200 (i.e. 20 x 10).
- Before saving the file, select all the layers and move the fracture pattern to a new position such that no line coordinate is less than 0 on the x-axis or greater than 0 on the y-axis. This prevents the fracture pattern from being displayed upside down in JAWS.

It is not required, but if the user wants data analysis for each fracture set, it is recommended that each fracture set be in separate layers. Also, if the user needs the coordinates for each fracture trace, JAWS creates a text file **(C:\Frac\adobedata.txt)** of the line coordinates for each straight-line segment of the Adobe Illustrator file. This text file is similar to Table A1.

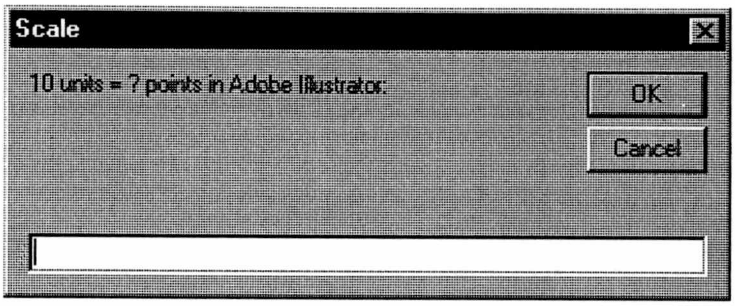

Figure A2. Allows the user to enter the scale factor.

3.1.2 Text File

If opening a text file that contains fracture coordinates of a digitized fracture pattern (Figure A3), the file must be in the same format as Table A1. The first four rows must contain the title of the layer. After all the coordinates for a particular layer have been entered, the next four lines must contain the title of the next layer.

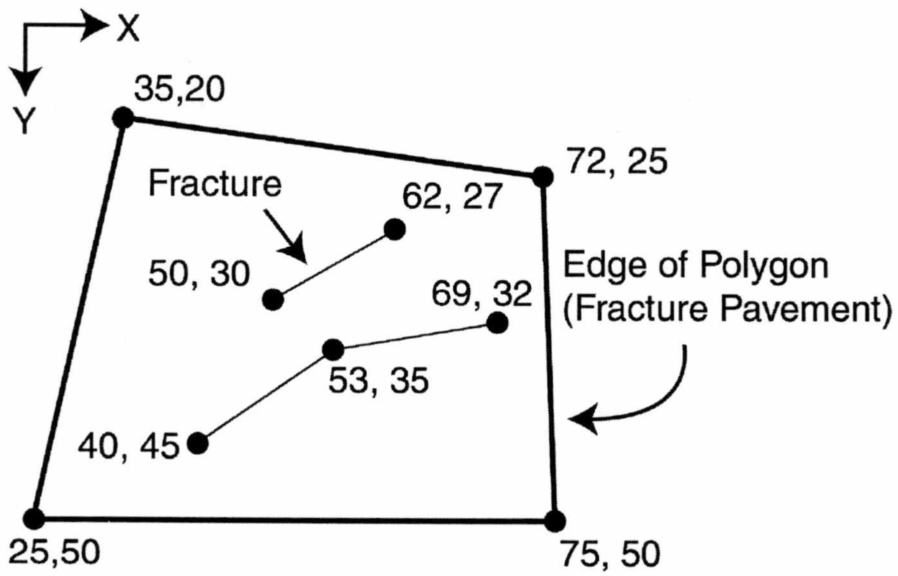

Figure A3. Example of a digitized fracture pavement containing 2 fractures (i.e. Set 1).

Table A1. Example text file using coordinate data from Figure A3.
* Must enter the title of the layer 4 times

Polygon	Layer Title *
Polygon	
Polygon	
Polygon	
35,20	Polygon (Fracture Pavement) Coordinates
25,50	
25,50	
75,50	
75,50	
72,25	
72,25	
35,20	
Set1	Fracture Set 1 Layer Title *
Set1	
Set1	
Set1	
50,30	Polyline (Fracture) Coordinates
62,27	
40,45	
53,35	
53,35	
69,32	

Note: Make sure that the rows containing the title of the layer contain no spaces; Also make sure that the total number of lines in the text file does not exceed 10,000.

3.2 *Synthetic Data*

For synthetic data, the user enters the **"density"** (Number of Fractures), **mean tracelength**, and **mean orientation** for each fracture set (Figure A4). The next three screens allow the user to enter data for fracture sets 2, 3, and 4 respectively. Use the **Next** button to bypass any screens that contain no data.

3.2.1 Mean Density

Mean density refers to the mean number of fracture centers per unit area that will be plotted in the sampling window. The area of the sampling window will be entered at a later stage in the program.

3.2.2 Mean Tracelength

For mean tracelength, there are three length distributions to choose from.

1. A fixed fracture length
2. A uniformly distributed fracture length that is centered on the mean +/- the range
3. An exponential distribution that is centered on the mean

3.2.3 Mean Fracture Orientation

For the mean fracture orientation, there are three distributions to choose from.

1. A fixed orientation
2. A uniform distribution that is centered on the mean +/- the range
3. A triangle distribution that is centered on the mean +/- the range

3.3 *Manual Data*

If the user wants to plot fracture traces by entering the data manually (Figure A4), the user must input the number of fractures using the **# of Fractures** option under the **Options** menu. The user will enter x, y-coordinates of the fracture center, fracture length, and fracture orientation.

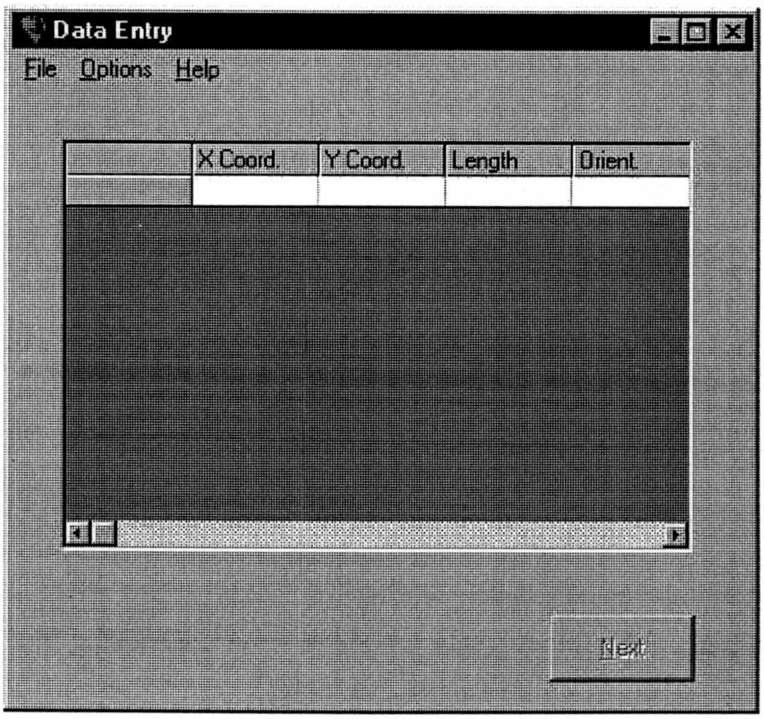

Figure A4. Allows the user to enter fracture data manually.

4.0 DATA ANALYSIS

Once the data has been entered or loaded into JAWS, the next step is to analyze the data. For synthetic traces, fractures are plotted in a generation region using a Poisson point process. The area that is actually sampled (sampling region) is a subset of the generation region. The size of this sampling region is chosen to eliminate edge affects. For natural fracture patterns, fractures are only plotted in the sampling region.

4.1 *Plotting*

4.1.1 Synthetic Fracture Data

To plot synthetic fracture traces, choose **Fractures** or **Fractures and Centers** option under the **Plot** menu (Figure A5). The user must then enter the dimensions of the sampling region (large white box on the bottom half of the screen). The dimensions of the sampling region are unitless. To change the dimensions of the sampling region, choose the **Dimensions** menu option.

4.1.2 Natural Fracture Data

To plot natural fracture patterns, choose **Fractures** option under the **Plot** menu (Figure A5). The optimum dimensions of the sampling region are chosen by the program based upon the programs knowledge of the fracture coordinates and the scale factor (previously entered). (**NOTE:** If a scale factor of 200 points equals 10 meters was entered, then the dimensions of the sampling region are in meters.) The user then enters the **area** of the fracture pavement. (**Hint**: I have found that the **area** can be easily calculated in **Canvas.**)

4.1.3 Scanlines/Windows

Once the data has been plotted, the user has the option of plotting a **straight scanline** or **circular scanline/window** (Figure A5).

4.1.3.1 Straight Scanlines

After selecting **Linear** from the **Scanline** pull-down list, the user must enter the number of straight scanlines choosing the **# of Scanlines** option under the **Options** menu (Figure A6). Then, the x, y-coordinates of the center of the scanline, scanline length, and scanline orientation must be entered (**Note**: If using multiple straight scanlines, all the scanlines must have the same orientation). Pressing the **Next** button brings back the main form. The scanline is displayed by choosing the **Scanline** option under **Plot**. For natural fracture pavements, the **FIRST** scanline must be placed completely within the fracture pavement.

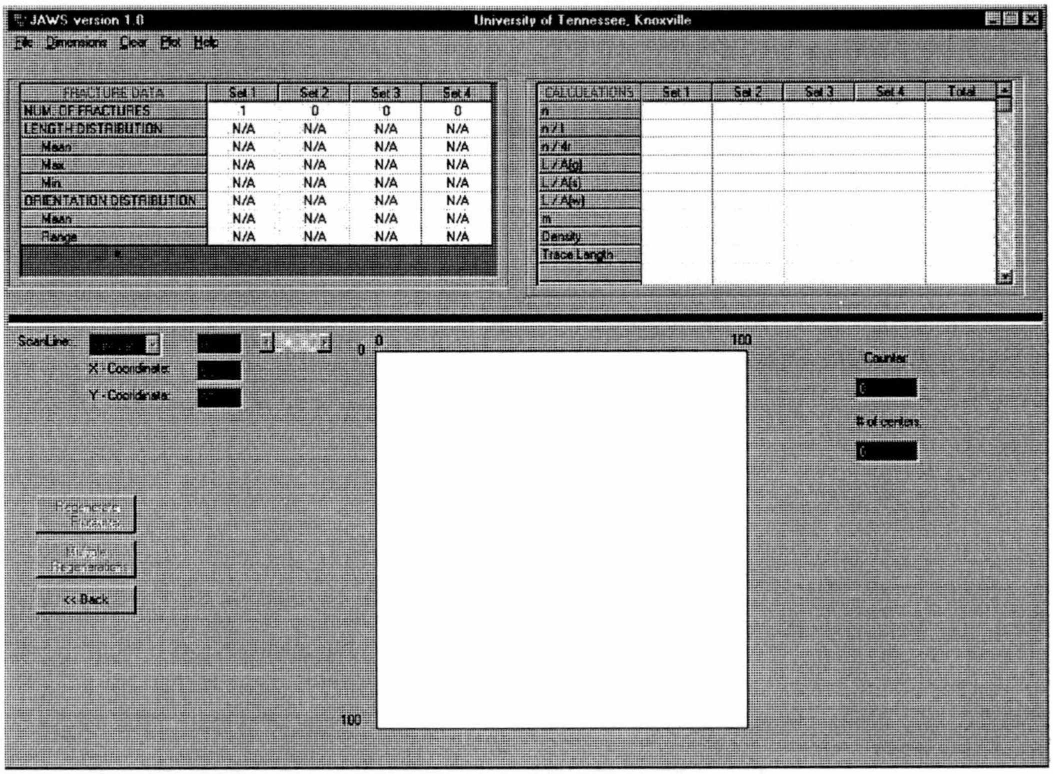

Figure A5. Allows the user to plot and analyze fracture data

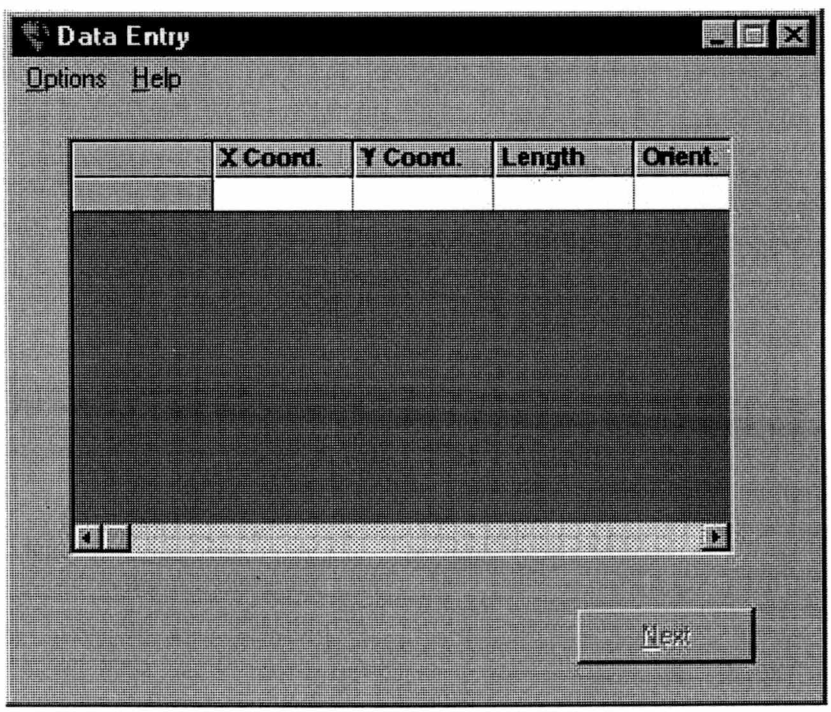

Figure A6. Allows the user to input data for straight scanlines

4.1.3.2 Circular Scanline/Window

After selecting **Circular** from the **Scanline** pull-down list, the user must enter the radius and x, y- coordinates of the center of the circular scanline/window. The next step is to choose the **Scanline** option under **Plot**. For natural fracture pavements, the **FIRST** scanline must be placed completely within the fracture pavement.

4.2 Automating Analysis (Synthetic Fractures)

4.2.1 Regenerate Button (Straight & Circular Scanlines/Windows)

Synthetic fracture traces can be regenerated by pressing the **Regenerate** button (Figure A5) (**Note**: the **Regenerate** button can only be pressed **500** times). This option fixes the position of the scanline, but generates a new synthetic fracture pattern each time the Regenerate button is pressed.

4.2.2 Multiple Regenerate Button (Straight & Circular Scanlines/Windows)

Performs the same task as the Regenerate button, except this option allows the user to enter the number times to regenerate the fracture pattern.

4.2.3 Random Scanline (Circular Scanlines/Windows)

To analyze the fracture pattern by "randomly" (i.e. circles are uniformly distributed on the fracture pattern) positioning the scanlines/windows on the pavement, the user must choose the **Random Scanlines→Synthetic Fractures** option under the **Plot** menu. The user must then specify the number of circles to be completely contained within the pavement.

The computer then generates uniformly distributed the center coordinates of the circular scanlines/windows, and only analyzes those scanlines/windows that are completely contained within the fracture pattern. This process is repeated until the specified number of scanlines/windows, entered by the user, is achieved.

4.3 Automating Analysis (Natural Fracture Patterns)

4.3.1 Random Scanlines (Circular Scanlines/Windows)

To rapidly analyze a natural fracture pattern, the scanlines/windows need to be uniformly distributed over a fracture pattern. To do this, the user must first specify the radius of the circle. Then, under the **Plot** option, choose the **Random Scanlines→Natural Fractures** option. The user must then specify the number of circles to be completely contained within the pavement.

The computer then generates uniformly distributes the center coordinates of the circular scanlines/windows, and only analyzes those scanlines/windows that are completely contained within the fracture pattern. This process is repeated until the specified number of scanlines/windows, entered by the user, is achieved.

4.3.2 Output for Contouring (Circular Scanlines/Windows)

If the user wants data that can be used for contouring, the **Output for contouring** option under the **Plot** menu can be selected. The user only needs to specify the radius of the circular scanline. This allows the computer to plot a grid of circular scanlines whose centers are one radius apart. Only data for those circular scanlines completely contained within the pavement are written to a file.

5.0 CALCULATED PARAMETERS:

The following list defines the mathematical parameters that appear under the Calculations table in the upper right-hand corner (Figure A5).

- **n** refers to the number of fractures intersecting either a straight scanline or the circumference of a circular scanline/window.
- **n / l** refers to the Terzaghi (Terzaghi, 1965) corrected fracture intensity as determined from a straight scanline, where **n** is the "weighted" number of fractures intersecting the scanline and **l** is the length of the scanline. The weighting factor for each fracture intersected (i.e. **n**) is csc θ, where θ is the angle between scanline and the fracture. The sum of these "weighted" fractures gives a "weighted" **n**.
- **n / 4r** refers to the intensity estimator for circular scanlines (Mecke, 1981; Stoyan et al., 1995; Mauldon et al, 1999), where **n** is the number of fracture traces intersecting the circular scanline and **r** is the radius of the circular scanline.
- **L / A(g)** represents the input intensity into JAWS. For a particular set, this is determined using the equation (ρ x L) / A, where ρ is the density of that fracture set, L is mean length of that fracture set, and A represents the area of the sampling region.
- **L / A(s)** refers to the intensity of the sampling region. This is determined by dividing the total length of fracture traces inside the sampling region by the area of the sampling region.
- **L / A(w)** refers to the intensity estimate using circular windows, where **L** is the length of fracture traces inside the circular window, and **A** is the area of the circular window.

- **m** refers to the number of fracture endpoints inside the circular window
- **Density** refers to an estimate of the mean number of fracture centers per unit area determined from circular windows. This is determined using the equation $m/2\pi r^2$ (Mauldon, 1998; Mauldon et al., 1999), where *m* is the number of fracture endpoints inside the circular window, and *r* is the radius of circular window.
- **Tracelength** refers to an estimate of the mean fracture tracelength determined from circular windows. This is determined using the equation $(n/m)\times(\pi r/2)$ (Mauldon, 1998;Zhang and Einstein, 1998; Mauldon et al., 1999), where *n* is the number of fracture traces intersecting the perimeter of the circular window, *m* is the number of fracture endpoints inside the circular window, and *r* is the radius of the circular window. **NOTE: TO PREVENT A COMPUTER OVERFLOW ERROR, THIS PROGRAM RECORDS AN ESTIMATED TRACELENGTH OF 0 WHEN $m = 0$ (i.e. ESTIMATED TRACELENGTH EQUALS INFINITY).**

Note: Data analysis that appears in this table is also written to C:\Frac\ FracSet1.txt, ... FracSet4.txt.

6.0 DATA OUTPUT

All calculations of fracture data are written as comma delimited text to C:\Frac\ FracSet1.txt, ..., C:\Frac\FracSet4.txt. Each file refers to data for fracture set 1, ..., fracture set 4 respectively.

6.1 Synthetic Traces

6.1.1 Circular Scanlines/Windows

A header will be displayed showing the number of fractures input for that particular set; its mean, maximum, and minimum length plus the length distribution; its mean orientation plus the orientation distribution; the radius of the circular scanline/window; and the area of the sampling region.

For the fracture calculations, **Circle X** and **Circle Y** refers to the center coordinates of the circular scanline, **n** refers to the number of fractures intersecting the circumference of the circle, **m** refers to the number of fracture endpoints inside the circle, **n / 4r** refers to the intensity estimate of fracture intensity determined from circular scanlines, **L / A(w)** refers to the intensity estimate determined from circular windows, **L / A(g)** refers to the true intensity of the fracture population, **L / A(s)** refers to the intensity of the sampling regions, **Density** refers to the estimate of mean fracture density determined using circular windows, and **Tracelength** refers to the estimate of the mean fracture tracelength determined using circular windows.

6.1.2 Straight Scanlines

A heading similar to the one used for circular scanlines/windows is used, except the information on circle radius is replaced by the length and orientation of the straight scanline.

For fracture calculations, **Corrected** refers to Terzaghi corrected number of fracture intersections, **Uncorrected** refers to the actual number of the fractures intersecting the straight scanline, **n / l** refers to the Terzaghi corrected fracture intensity, **L / A(g)** refers to the true intensity of the population, and **L / A(s)** refers to the intensity of the sampling region.

6.2 Natural Fracture Patterns

6.2.1 Circular Scanlines/Windows

The header contains only the number of fractures in that particular set, the radius of the scanline/window, and the area of the fracture pavement. If the user opened a natural fracture pattern from an Adobe Illustrator file, the radius is also given in points. This allows the user to plot this circle in Adobe Illustrator (if they so desire).

Fracture data that is output to the text file using the format listed in section 6.1.1. The only exception is the information on the true intensity of the population is not available. Also, if the fracture pattern was opened from an Adobe Illustrator file, the location of the center coordinate of the circular scanline/window is given in points, otherwise the coordinates are in map units. By giving the coordinates in points, the user can now plot this circle in Adobe Illustrator (if they so desire). If the circular scanline/window coordinates want to be converted back into map units, this is achieved by dividing the circle coordinates by 1/10th the scale factor entered in section 3.1.1.

If the user is using the **Output for Contouring** option under the **Plot** menu. Data on the location (also given in points) and radius (also given in points) of the circle, and the intensity of fracture set 1,…, fracture set 4 are written as comma delimited text to **C:\Frac\Contour.txt**.

6.2.2 Straight Scanlines

A heading similar to the one used for circular scanlines/windows is used, except the information on circle radius is replaced by scanline length and orientation.

Fracture data that is output to the text file using the format listed in section 6.1.2. The only exception is the information on the true intensity of the population is not available.

6.3 Save As

Any image in the sampling region can be saved as a bitmap using the **Save As** option under **File**.

6.4 Save Fractures

This option allows the user to save a synthetic fracture pattern as a text file. This allows the user to load this same pattern for later analysis. For each saved pattern, the user will want to keep a record of the input parameters (i.e. dimensions and area of sampling region, fracture density, fracture tracelength, fracture orientation, etc.).

To load this pattern, follow the instruction in section 4.1.2.

7.0 REFERENCES CITED

Mauldon, M., 1998. Estimating mean fracture tracelength and density from observations in convex windows: Rock Mechanics and Rock Engineering, v. 31, p. 201-216.

Mauldon M., M.B. Rohrbaugh Jr., W.M. Dunne and W. Lawdermilk, 1999, Fracture intensity estimates using circular scanlines, in B. Amadei, R.L. Kranz, G.A. Scott and P.H. Smeallie eds., Proceedings of the 37th US Rock Mechanics Symposium: Rock Mechanics for Industry: Rotterdam, Balkema, p. 777-784.

Mauldon, M., M.B. Rohrbaugh Jr., W.M. Dunne and W. Lawdermilk, 1999, Estimators for mean fracture tracelength and density using circular windows, in B. Amadei, R.L. Kranz, G.A. Scott and P.H. Smeallie eds., Proceedings of the 37th U.S. Rock Mechanics Symposium: Rock Mechanics for Industry: Rotterdam, Balkema, p. 785-792

Mecke, J., 1981, Formulas for stationary planar fibre processes III - intersections with fibre systems: Mathematische Operationsforschung und Statistik. Series Statistik, v. 12, p. 201-210.

Stoyan, D., W.S. Kendall and J. Mecke, 1995, Stochastic geometry and its applications, 2nd edition: New York, John Wiley and Sons, p. 286-296.

Terzaghi, R.D., 1965. Sources of error in joint surveys: Geotechnique, v. 15, p. 287-304.

Zhang, L. and H.H. Einstein, 1998, Estimating the mean tracelength of rock discontinuities: Rock Mechanics and Rock Engineering, v. 31, p. 217-234.

APPENDIX B

USE OF COMPACT DISC

The compact disc located in the back pocket contains a Setup.exe of JAWS version 1.0 (located in the JAWS\Executable folder), program code (located in the JAWS\JAWS Code folder), a help file (located in the JAWS\Help folder), and sample natural fracture pavements with a file containing information on pavement area and scale conversion factors (located in the JAWS\Pavement folder). For information on how to use the program, see Appendix A or the help file. The compact disk is only for use on IBM compatible computers.

VITA

Melvin Bruce Rohrbaugh Jr. was born in Petersburg, West Virginia on May 29, 1975. He is the son of Melvin B. and Josephine Rohrbaugh. He attended the Grant County Public School system and graduated from Petersburg High School in 1993. He attended West Virginia Institute of Technology from 1993 to 1995 were he was a Computer Science major. After realizing that geology was his true love, he transferred to West Virginia University to pursue a degree in Geology. He graduated *Magna Cum Laude* in August, 1997 with a Bachelor of Science degree in Geology. He entered the Master's program in Geology at The University of Tennessee, Knoxville in August, 1997 and focused his studies on structural geology. He officially received the Master of Science degree in May, 2000. He accepted an internship with Exxon, which begins in April, 2000.